Forecasting Research Division
Technical Report No. 59

THE 1992 AUTUMN EQUINOCTIAL DOWNPOUR: CAUSES AND NWP MODEL ASSESSMENT

by

J.R. Grant, M.J. Bader, C.A. Wilson, T. Davies and S.P. Ballard

NOVEMBER 1993

FORECASTING RESEARCH TECHNICAL REPORT NO 59

THE 1992 AUTUMN EQUINOCTIAL DOWNPOUR: CAUSES AND NWP MODEL ASSESSMENT

by

J R Grant, M J Bader, C A Wilson, T Davies and SP Ballard*
Forecasting Research Division

*now at Joint Centre for Mesoscale Meteorology, APR Division, Reading University

November 1993

Forecasting Research division
Meteorological Office
London Road
Bracknell
Berkshire, RG12 2SZ
United Kingdom

NOTE: This paper has not been published. Permission to quote from it must be obtained from the Director of the above Meteorological Office Division.

CONTENTS

1. INTRODUCTION
2. RAINFALL
3. SYNOPTIC DEVELOPMENTS
4. THE LIMITED AREA MODEL (LAM) FORECASTS

- 4.1 RAINFALL
- 4.2 WET BULB POTENTIAL TEMPERATURE (WBPT) AT 850 hPa AND RELATIVE HUMIDITY
- 4.3 UPPER WINDS, VORTICITY AND ASCENT
- 4.4 DIAGNOSIS USING POTENTIAL VORTICITY (PV)
- 4.5 MODEL EXPERIMENTS

5. MESOSCALE MODEL FORECASTS
   - 5.1 INTRODUCTION
   - 5.2 OUTPUT FROM DIFFERENT RUNS

6. CONCEPTUAL MODEL

7. LESSONS FOR FORECASTERS

REFERENCES

ACKNOWLEDGEMENTS

FIGURE LEGENDS

APPENDIX: MESOSCALE MODEL FORECASTS: A SENSITIVITY STUDY

A.1 INTRODUCTION
A.2 ORIGINAL OPERATIONAL MESOSCALE FORECASTS
A.3 LAM AND NEW MESOSCALE MESOSCALE MODEL FORECASTS
A.4 IMPACT OF DATA AND DATA ASSIMILATION
A.5 SENSITIVITY TO CONVECTION SCHEME
A.6 SENSITIVITY TO HORIZONTAL DIFFUSION
A.7 INITIAL OPERATIONAL VERSION OF NEW MESOSCALE MODEL
A.8 COMPARISON OF INSTANTANEOUS SURFACE PRECIPITATION RATES
A.9 CONCLUSIONS

REFERENCES

1. INTRODUCTION

Precipitation on the northern side of a slow-moving cut-off upper low can be heavy and persistent, giving rise to large accumulations. In such situations, NWP models have recently predicted the precipitation inaccurately. An example occurred on the evening and night of 22nd to 23rd September 1992 when heavy rain fell over southern and eastern England. In spite of the poor guidance from the UK limited area model (LAM) in this case, the forecasts issued were reasonable, showing the success of the 'man-machine mix'. Interestingly, the French Peridot model also failed to predict the rain over England (Senesi, personal communication).

2. RAINFALL

The distribution and intensity of rainfall from the UK weather radar network are presented in Fig. 1. In the evening of the 22nd, there were areas of heavy, showery rain over parts of southern and eastern England (Fig. 1a). In places, instantaneous rates exceeded 32 mm per hour.

This showery rain then became more widespread during the evening (Fig. 1b). Cells of heavy rain moved west-northwestwards at up to 17 knots. After 21 UTC, a well-organised band developed, containing pockets of rain with rates as high as 32 mm/hr (Fig. 1c). About this time a rotation became apparent in the band as cells of heavier rain still moved to the west-northwest at around 17 knots over the Wash, whilst over Wiltshire the cells moved to the east-southeast at 14 knots. The band, which had a sharp western edge, thus pivoted slowly anti-clockwise (Fig. 1d). By 06 UTC, the heaviest rain was confined to north-east England while the rain in the south had become much lighter (Fig. 1e).

In the 24 hour period to 09 UTC on 23rd, rainfall totals exceeded 40 mm over a large area (Fig. 2), with spot values close to 100 mm. An example of the impact of these high totals in East Leicestershire is shown in Fig. 3.

3. SYNOPTIC DEVELOPMENTS

This cloud and rain over England were associated with a developing shallow surface low which moved slowly north over south-east England into the southern North Sea (Fig. 4) on the north-eastern flank of an upper vortex V (Fig. 5). Ahead of the cold front over the Continent, warm, moist unstable air was advected northwestwards over the southern North Sea into eastern England.

The satellite pictures show the evolution clearly. The showery rain on the afternoon and early evening of the 22nd fell from cloud D (Fig. 6a). (The swirl of cumuliform cloud over France reveals the upper vortex. Also shown are large cumulo-nimbus on the eastern flank of the vortex giving exceptionally heavy rain and widespread flooding over south-eastern France (Benech et al 1993). Debris from these clouds moved north towards Holland).

A small area of cloud E1 (Fig. 6a), whose tops were warmer than the cloud to the east, grew together with other cloud G (Fig. 6b) and merged with D forming a continuous cloud area E2 whose tops continued to cool (Figs 6c, 6d). During this evolution, the rain from these cloud areas became more widespread. A dry slot (Fig. 6e) in the water vapour image on the cold side of the jet on the eastern side of the upper vortex V separated E2 from the Continental cirrus plume. This evolution is a sign of cyclogenesis (see Chapter 5 of 'Images in Weather Forecasting').

4. THE LIMITED AREA MODEL (LAM) FORECASTS

4.1 RAINFALL

The poor forecast in question was run from data at 00 UTC on 22nd September. This will be called Run A. The LAM forecast the rain at least 6 hours too late.

Fig. 7a shows that the LAM only produced significant dynamic rain over East Anglia, the East Midlands and south-east England after 00 UTC on 23rd. The largest totals in the period from 12 UTC on 22nd to 06 UTC on 23rd did not exceed 20 mm (Fig. 8a) anywhere over England. Even bearing in mind the resolution of the model, these totals did not match the 24 hourly totals in Fig. 2. (This evolution was also consistent with forecasts on the 21st).

The evolution from the LAM run of 12 UTC on 22nd September (Run B) was much better (Fig. 7b). It forecast more rain over England much earlier, including showers in the evening, with highest totals of 41 mm for the 18 hour period discussed above (Fig. 8b). Such values would suggest locally heavy falls of rain. (However, the rain was still forecast a little too late and to last for too long). The surface depression centre became defined 6 hours earlier than in Run A.

In the following sections, reasons for the poor forecast in Run A will be discussed using Run B as a control.

4.2 WET BULB POTENTIAL TEMPERATURE (WBPT) AT 850 hPa AND RELATIVE HUMIDITY

The 850 hPa wet bulb potential temperature (WBPT) evolves differently in Runs A and B.

Run B has a tongue of warm, moist air extending from the North Sea, south-westwards over England (Fig. 8b) by 18 UTC on the 22nd. However, the hand-drawn analysis based on the observations shows that the tongue is already well established at 12 UTC (Fig. 9) compared with that in Run A (Fig. 10). In Run A, the tongue over England is far less developed (Fig. 8a) throughout the period from 12 UTC on 22nd to 06 UTC on 23rd.

These differences are also reflected in the fields of relative humidity. At 12 UTC on 22nd, the air over England was much drier at 700 hPa in Run A (Fig.11a) than Run B (Fig.11b). (Note that the relative humidity at 700 hPa was bogussed in Run B but a re-run without the bogus gave almost exactly the same evolution of the rainfall).

By 00 UTC on 23rd, a tongue of nearly saturated air extended from the North Sea over central England in Run B (Fig. 11d) but was fragmented in Run A (Fig. 11c). The pattern in Run B agrees much better with the cloud E2 on the satellite picture (Fig. 6d). Furthermore, Run B shows dry air (e.g., at 500 hPa (Fig. 12b)) over the southern North Sea, consistent with the dry slot on the water vapour image (Fig. 6e). This dry slot does not extend far enough north in Run A (Fig. 12a) because of the delayed cyclogenesis.

4.3 UPPER WINDS, VORTICITY AND ASCENT

The dominant feature is the upper vortex. At 12 UTC on 22nd, the 300 hPa height and wind fields from Runs A (Fig. 13a) and B (Fig. 13b) are almost identical. The axis of the upper trough is close to the meridian and winds are strongest on its eastern flank. The model's 300 hPa winds at this time over the Continent agreed to within a few knots of the observed winds in both Run A and Run B.

Although both runs predicted the north-eastward movement of the vortex, the evolutions differed slightly in detail. In Run B (Fig. 14b), the vortex moved a little faster and developed into a more rounded pattern by 00 UTC on 23rd than in Run A (Fig. 14a).

Evidence for Run B being more accurate than Run A is as follows.

> The radiosonde winds at 250 hPa show a well-defined veer and decrease over Spain and France on the 22nd (Fig. 15), marking the passage of a short wave trough. For example, at 00 UTC on 23rd, the observed wind of 185 degrees, 35 knots at Paris matched the pattern in Run B (Fig. 14b) better than in Run A (Fig. 14a) which still indicated a south-easterly wind. The upper trough was just behind cloud area E1 discussed in Section 3.
>
> Relative to the movement of the surface low (185 degrees 12 knots), Run B had by midnight produced a north-easterly wind at 300 hPa in the region of cloud E2 in Fig. 6d. This is consistent with the motion of E2. Such a velocity could not be derived from a 45 knot south-easterly wind produced in Run A.

A small but perhaps significant trough in a model upper wind field is often better located by the vorticity pattern and consequent areas of PVA identified. The positive vorticity advection (PVA) north of the vortex advected from the south over Eastern England can be clearly deduced from the sequence of vorticity maps from Run B (Fig. 16b), corresponding to the contour and isotach charts in Fig. 14b. Note in particular the movement of vorticity centre Q into East Anglia, ahead of which was localised mass ascent (Fig. 17b). In Run A, the vorticity patterns (Fig. 16a) at 12 and 18 UTC were very similar to Run B but at 00 UTC the vorticity maximum was still well to the south, only approaching south-east England by 06 UTC. Therefore, ascent was only produced after midnight (Fig. 17a); it was smaller in area and further east than in Run B.

Even though Run B was good, the detail was not quite correct. In particular, the winds on the forward side of the upper trough were too light. For example, at 00 UTC on 23rd, the radiosonde ascent at Uccle reported a wind of 165 degrees, 96 knots at 300 hPa. This is about 20 knots stronger than the forecast wind from Run B (Fig. 14b). The real vorticity and subsequent PVA are therefore likely to have been stronger than the model values; this may account for the slightly delayed development of the heavy rainfall in Run B.

The initial backing then veering of the observed 250 hPa winds at Hemsby between 00 and 06 UTC on 23rd, as the upper trough passes through, is very well marked (Fig 15). The actual wind direction does not, however, conform with either model run. It seems that the vortex filled and moved northeast rather faster than in the model forecast —hence the early observed onset of the westerly component to the winds and the cessation of rain earlier than the model runs predicted.

4.4 DIAGNOSIS USING POTENTIAL VORTICITY (PV)

Another way of looking at the evolution is by using potential vorticity (PV) (see e.g., Bluestein (1992)). PV is conservative for adiabatic processes so features can be followed over significant periods of time.

The PV maps from Runs A and B for 12 UTC on 22nd (Figs. 18a, 19a) are similar. There is a pronounced area of high PV over western France associated with the upper vortex. In both figures, there is a gradient of 850 WBPT to the east of the PV anomaly.

Although at this time the patterns of PV and 850 WBPT appear similar in both runs of the model, there are some subtle differences from which subjective inferences can be drawn relating to possible cyclogenesis. Development is more likely if a large upper PV anomaly can engage a low-level potential temperature anomaly e.g., at 850 hPa. The degree of development is dictated by the intensities and relative positions of the upper and lower level anomalies. Upper anomalies have a greater influence if the air in the lower troposphere is moist and unstable. In particular, the PV anomaly in the 12 UTC analysis of Run B is closer to the high values of 850 WBPT because the upper anomaly is a little further east and the warm, moist low-level air extended further westwards.

These differences are significant enough to infer that any development would be expected earlier from the patterns in Fig. 19a than from Fig. 18a. This is similar to the notion of development in a region of PVA approaching a low-level baroclinic zone. In this case, the PV anomaly is moving north-eastwards and development would be expected near X in Fig. 19a as the anomaly approaches the warm, moist air at low-levels from the south-west.

In both runs of the LAM, the PV anomaly moves north-east. However, the evolution in Run B (Fig. 19 b-e) is different in detail from Run A (Fig. 18b-f) for the following reasons.

The PV anomaly engages the high WBPT in the form of a tongue on its north-eastern side much earlier in Run B. The tongue is caused by relative advection of warm air south-westwards along its axis. The corresponding evolution in Run A is slower and weaker, the upper anomaly appearing to just reach the region of higher WBPT by 00 UTC on 23rd.

The lobe on the eastern side of the PV anomaly rotates anti-clockwise faster in Run B. The cyclogenesis takes place ahead of this northward moving lobe of high values, as theory predicts. Looked at in more detail, the rotation is faster near the centre of the anomaly than on the outside, the anomaly changing to a much more rounded pattern by 00 UTC on 23rd. By this time, there may be some feedback on the PV pattern from diabatic effects (e.g, the effects of precipitation).

The main conclusion from this analysis is that the early errors in Run A are such that the upper PV anomaly does not interact with the low-level warm air until several hours after that in Run B. Because the upper and lower anomalies have moved north-eastwards, the development takes place over the North Sea rather than over south-east England.

The question of whether differences in the upper level pattern (as perceived, for example, by the different shapes of the PV anomalies) were mainly responsible for the different forecasts or whether the properties of the air at low levels are important is addressed by running forecasts using different combinations of fields at upper and lower levels. These experiments are described in Section 4.5.

4.5 MODEL EXPERIMENTS

Fields valid at 12 UTC on 22nd at and above 700 hPa were transplanted with others below 700 hPa from a different run but valid at the same time.

The transplants were as follows.

(a) The top levels from the poor forecast (Run A), beginning at T+12, were transplanted on to the bottom levels from the control run (Run B), beginning at T+0. This transplant will be called $[\frac{\mathbf{00}}{\mathbf{12}}]$ and is equivalent to bogussing the poor run with a better representation of the structure at low levels.

(b) The top levels from the control run (Run B), beginning at T+0, were transplanted on to the bottom levels of the poor run (Run A), beginning at T+12. This transplant will be called $[\frac{\mathbf{12}}{\mathbf{00}}]$ and is equivalent to bogussing the good run with a poorer representation of the structure at low levels.

The 6 hourly accumulated precipitation and 850 WBPT patterns valid at 18, 00 and 06 UTC from these transplants (Figs 20a and 20b) are compared with those from Runs A and B (Figs 8a and b).

The top panel (Fig. 20a) is transplant $[\frac{\mathbf{00}}{\mathbf{12}}]$ and the bottom panel (Fig. 20b) transplant $[\frac{\mathbf{12}}{\mathbf{00}}]$. Figs 7 and 21 show surface pressure and instantaneous rainfall rate for the same runs as shown in Figs 8 and 20.

The results are summarised in Table 1.

SL is an abbreviation for the surface low. Rainfall totals, R, are for the 6 hour period ending at times stated. The values in the bottom row are observed rainfall totals, taken from Fig. 23, and averaged over the equivalent of 3x3 grid squares of the LAM. These values can be compared with forecast values from the model.

TABLE 1 COMPARISONS BETWEEN FORECASTS OF THE OPERATIONAL RUNS AND TRANSPLANTS

RUN	VALID AT 22/1800	VALID AT 23/0000	VALID AT 23/0600
RUN B (CONTROL) **(Fig. 8b, 7b)**	Convective rain, some heavy, over large part of Central and Southern England. R: up to 4 mm. SL: centre over Eastern England.	Dynamic rain organised in band 150 km wide over eastern England. R: 4 to 6 mm. SL: slight filling; centre just off Wash.	Dynamic rain organised in band 120 km wide over Eastern England. R: up to 20 mm. SL: continued slow drift to NE; little pressure change
TRANSPLANT **[00/12]** **Figs 20a, 21a** 850 WBPT very similar to RUN B throughout.	Convective rain covers similar area to Run B. R: up to 4 mm, similar to Run B SL:centre as in Run B.	Convective rain but no dynamic rain. R: up to 1 mm. SL: slight filling; centre just south of Wash.	Area of dynamic rain similar to Run B. R: up to 16 mm. SL: little change; centre over Wash. Not as well defined as in Run B.
RUN A **Figs 8a, 7a**	Only a little convective rain, mainly in south-east England. R: up to 1 mm. Slack pressure gradient.	Hardly any rain. R: up to 1 mm. Shallow trough over southern North Sea.	Dynamic rain organised in band up to 180 km wide over E. Anglia, i.e. further east than **[00/12]** R: up to 8 mm. SL: Deepening; centre southern North Sea.
TRANSPLANT **[12/00]** **Figs 20b, 21b** 850 WBPT very similar to RUN A throughout.	Convective rain limited to Southern England. R: 1 to 2 mm. SL: Southern North Sea.	Isolated areas of convective and dynamic rain. R: up to 2 mm. SL: slight filling; centre in Southern North Sea.	Dynamic rain in band up to 120 km wide. R: only 2 to 5 mm. SL: slight filling; centre in Southern North Sea.
Average of observed rainfall totals over 150 km by 150 km. square.	4 mm.	20 mm.	17 mm.

In both transplants, the dynamic rain over Eastern England is forecast later than in Run B and the surface low is not sufficiently well defined at 00 UTC on 23rd. However, there are aspects of transplant [$\frac{00}{12}$] which are handled better than transplant [$\frac{12}{00}$]. In [$\frac{00}{12}$], there is more convective rain at 18 UTC (in agreement with the radar picture (Fig. 1a)) and the dynamic rain at 06 UTC is heavier. [$\frac{12}{00}$] probably has more realistic upper forcing than [$\frac{00}{12}$] but not enough moisture at low levels and instability to produce the correct amounts of rain. The [$\frac{00}{12}$] transplant probably has enough moisture at low levels and instability but has to wait for the upper level trigger to initiate ascent. In neither transplant was the upper forcing and warm air at low levels properly coupled. However, in Run B, the stronger coupling accelerated development.

The main conclusion from this experiment is that the forecast was influenced by warm air at low levels as well as the errors in the upper forcing. The failure in the Run A was probably due to insufficient warm, moist air at low levels and the late arrival of an upper level trigger to initiate ascent.

The poor representation of warm air at low levels at 12 UTC on the 22nd in Run A does not appear to be caused by a lack of observations in key areas or a problem in data assimilation because the low-level analysis of the LAM at 00 UTC on the 22nd fits the observations satisfactorily. One reason could be that, in the model forecast, insufficient warm air was advected from the east over southern England because the circulation around the depression was not strong enough.

5. MESOSCALE MODEL FORECASTS

5.1 INTRODUCTION

In this section, forecasts from the original UK Met Office non-hydrostatic mesoscale model, OMM, and the new mesoscale model (NMM), which is a high resolution version of the UK Met Office's Unified Model, are presented. An historical background of the models is given in the Appendix. The forecasts include accumulations of precipitation for six hour periods and should be compared with the observed accumulations (Fig. 23).

The results from the LAM given here are with new physics as opposed to the results given in the other sections which are operational (i.e. before the modified physics was introduced on 27th April 1993). The forecasts are very similar, except that the LAM with new physics produces slightly higher rainfall accumulations in this case.

The full mesoscale assimilation scheme was used for NMM forecasts from 06 UTC on 22nd September 1992 for direct comparison with the OMM. Forecasts from the NMM were also run from the 00 and 12 UTC LAM analyses to test the impact of the higher NMM resolution on the precipitation forecasts.

5.2 OUTPUT FROM DIFFERENT RUNS

(a) Runs from 00 UTC on 22nd

The NMM forecasts (Fig. 22b) were similar to the solution from the LAM (Fig. 22a). The NMM did produce rain but it was not early enough and the distribution did not conform with the observations (Fig. 23). (The OMM only ran to T+18 and so did not cover the period of interest. It is therefore not discussed here. Forecasts from the LAM and NMM were also run from the 00 UTC analysis from the *global* model and produced better results than from the 00 UTC LAM analysis. To investigate this further, it may be worth comparing the LAM and global analyses for 00 UTC.)

(b) Runs from 12 UTC on 22nd

The forecasts from the NMM run at 12 UTC were similar to the LAM (compare Fig. 24a with Fig. 24b) but the accumulations in the NMM were higher especially during the period of mostly convective rainfall between 18 and 24 UTC on 22nd, comparing well with the observations (Fig. 23). It is interesting to note that the tongue of high WBPT at 850 hPa which extends south-westwards from the North Sea is slightly warmer in the NMM than in the LAM at 00 UTC. This shows that the NMM has probably captured the warm conveyor belt W2 (described in Section 6) better than the LAM. Also the tendency for heavier rain is enhanced because of the higher WBPT at low levels.

This result shows that the representation of the atmospheric processes on a smaller scale can successfully fine-tune the forecasts from the LAM, given a reasonable framework of larger scale processes.

(c) Runs from 06 UTC on 22nd

The results from both versions of the mesoscale model, OMM (Fig. 25) and NMM (Fig. 26b), run at 06 UTC on 22nd gave some useful detail on the rainfall distribution of the 06 LAM (Fig. 26a). Although the distribution of the highest accumulations from the LAM were reasonable,

the totals were too low. (It is interesting to note that the WBPT at 850 hPa over England was higher than that from the LAM at 00 UTC but the accumulations were still too low.)

The OMM gave good indications of expected high accumulations in each of the six hour periods (Fig. 25). It successfully forecast the distribution of the peak accumulations between 12 and 18 UTC but the amounts were possibly overdone with maximum values of about 55 mm compared with observed values of 30 - 40 mm. The locations of the peak accumulations were not so good later on, being slightly too far north and west between 18 and 24 UTC and too far west and south between 00 and 06 UTC. Unfortunately, the model under-predicted the precipitation in the south-east and East Anglia. The forecast did not predict the pivoting of the precipitation band after midnight and kept the rain too far west and south than in reality.

The NMM gave a good indication of expected high rainfall accumulations (Fig. 26b). In all periods, accumulations were significantly higher than the LAM (Fig. 26a). The location of some of the peak values in the later stages of the forecast were well predicted. However, between 12 and 18 UTC, the accumulations were significantly lower than the OMM and the observations, possibly indicating increased problems with spin-up in the precipitation forecasts for the NMM compared with the OMM. The location of the rainfall was slightly better in the NMM than the OMM as it spread the rain slightly further east. However, neither model spread the area of significant accumulations far enough into East Anglia.

The solutions are sensitive to the initial data, parametrization of convection and horizontal diffusion. Results of experiments are presented in the Appendix.

The main conclusion is that although the detail is not quite correct, the 06 UTC mesoscale models did provide a useful early signal that heavy rain was probable in some areas of England, especially before 00 UTC on the 23rd - improving the forecast from the 06 UTC LAM.

6. CONCEPTUAL MODEL

The main airflows at 00 UTC on 23rd relative to the surface low (which moved from 185 degrees at 12 knots) are shown in Fig. 27. The conceptual model was derived from cloud patterns on the animated satellite images, isentropic analyses using the radiosonde observations and diagnostics from Run B.

The heavy rain from cloud E2 on Fig. 6d was associated with rapidly ascending air within a warm conveyor belt W2, represented by the tongue of high WBPT at 850 hPa extending south-westwards from the southern North Sea (Fig. 9). The position of W2 relative to the surface cold front was supported by cross-sections over southern England from Run B of WBPT, wind components, vertical velocity and relative humidity. On the western flank of W2 was a deformation zone in the relative flow which restricted the spread of cloud and rain westwards.

In the Lagrangian frame of reference, the rainfall rates within W2 were not unusually large because the dew points in the warm air were not exceptionally high. However, since the relative velocity of air in W2 (from the north) over Eastern England approximately opposed that of the surface low (from the south), outbreaks of heavy rain were concentrated over one region for a long time, giving rise to locally very large accumulations.

The other warm conveyor belt, W1, over the North Sea was part of the flow of air brought northwards from southern Europe on the eastern flank of the upper vortex and capped by the cirrus outflow from thunderstorms over southern France. As far as could be ascertained, W1 remained at a nearly constant height as it moved northwards over the North Sea where it was still unstable enough to give several clusters of thunderstorms prior to 21 UTC.

A tongue of dry air was present aloft over the Low Countries and southern North Sea (Fig. 6e) and is seen at Hemsby (H in Fig. 27) above 600 hPa (Fig. 28).

It is possible that the initial development of convective cloud, especially the line of showers along the south coast (Fig. 1a) in the evening of the 22nd, could have been influenced by local topography. However, the main rain area was associated with the warm conveyor belt W2.

7. LESSONS FOR FORECASTERS

Forecasting the distribution and intensity of precipitation when an upper trough disrupts is often difficult because of uncertainty in development and organisation of the precipitation. Since precipitation areas often move slowly in these situations, there is the risk of locally large totals, especially in the summer half-year when the air may be warm and humid. (The same synoptic situation can produce locally heavy snow in winter).

The LAM provides the initial guidance but, in these situations, the rainfall accumulations may not be large enough because of the model resolution. The forecast from the Mesoscale model can add useful detail on the distribution and intensity of the rainfall. The model forecasts can be fine-tuned and the areas most at risk identified as other evidence, described in (a) to (d) below, becomes available.

(a) In some cases, an analysis of potential vorticity (PV) may help to identify the coupling of upper and lower anomalies better than traditional methods. Such analysis (especially if areas of high PV are collocated with dry tongues on water vapour imagery) may support existing guidance on cyclogenesis or provide an alternative scenario.

(b) The re-runs of the LAM described in Section 4.5 show that, in addition to the forcing from upper levels, small differences in WBPT at 850 hPa of only one or two degrees can significantly influence the timing and location of cyclogenesis. They can be spotted if the model's forecasts are carefully monitored against observations, especially if a pattern in the WBPT field (indicating, for example, a tongue of high values associated with the development of a warm conveyor belt) begins to emerge and is collocated with developing cloud on satellite imagery (see (d)). In this case, differences between forecast and observed WBPT became apparent 6 - 12 hours before the heavy rain.

(c) New areas of developing cloud can reveal a new ascending warm conveyor belt on the cold side of a frontal zone. Recognition of such cloud areas (normally some hours before the precipitation becomes widespread and heavy) is vital. These areas assume greater importance if situated ahead of positive vorticity advection or a positive PV anomaly. A conceptual model of the principal airflows can be applied as the appropriate cloud feature develops. Such models provide important information about the organisation (and therefore location and timing) of the rain.

(d) The hook on the cloud pattern of cyclogenetic archetypes is often associated with large precipitation totals (Young 1993), especially when the relative airflow in the warm conveyor belt giving rise to the hook (wrapping around the rear of the depression) opposes the velocity of the depression itself. Large totals over a particular area are then possible even though the air is not particularly warm and moist.

REFERENCES

Bader M J, Grant J R, Waters A J, Lilley R B E, Forbes G S, 1994 Images in Weather Forecasting. Cambridge University Press. To be published.

Benech B, Brunet H, Jacq V, Payen M, Rivrain J-C, Santurette P, 1993. La Catastrophe de Vaison-la-Romaine et des Violentes Precipitations de Septembre 1992: Aspects Meteorologiques. La Meteorologie, 8^{e} Serie, pp 72- 86.

Bluestein H B 1992 Synoptic-dynamic Meteorology in Mid-latitudes. Principles of Kinematics and Dynamics. Oxford University Press. (Vol 2).

Young M V 1993 Cyclogenesis: Interpretation of Satellite and Radar Images for the Forecaster. Met. Office UK Forecasting Research Technical Report No. 73..

ACKNOWLEDGEMENTS

Help from Gary Holpin, Ruth Lilley and Ewen MaCallum is gratefully acknowledged.

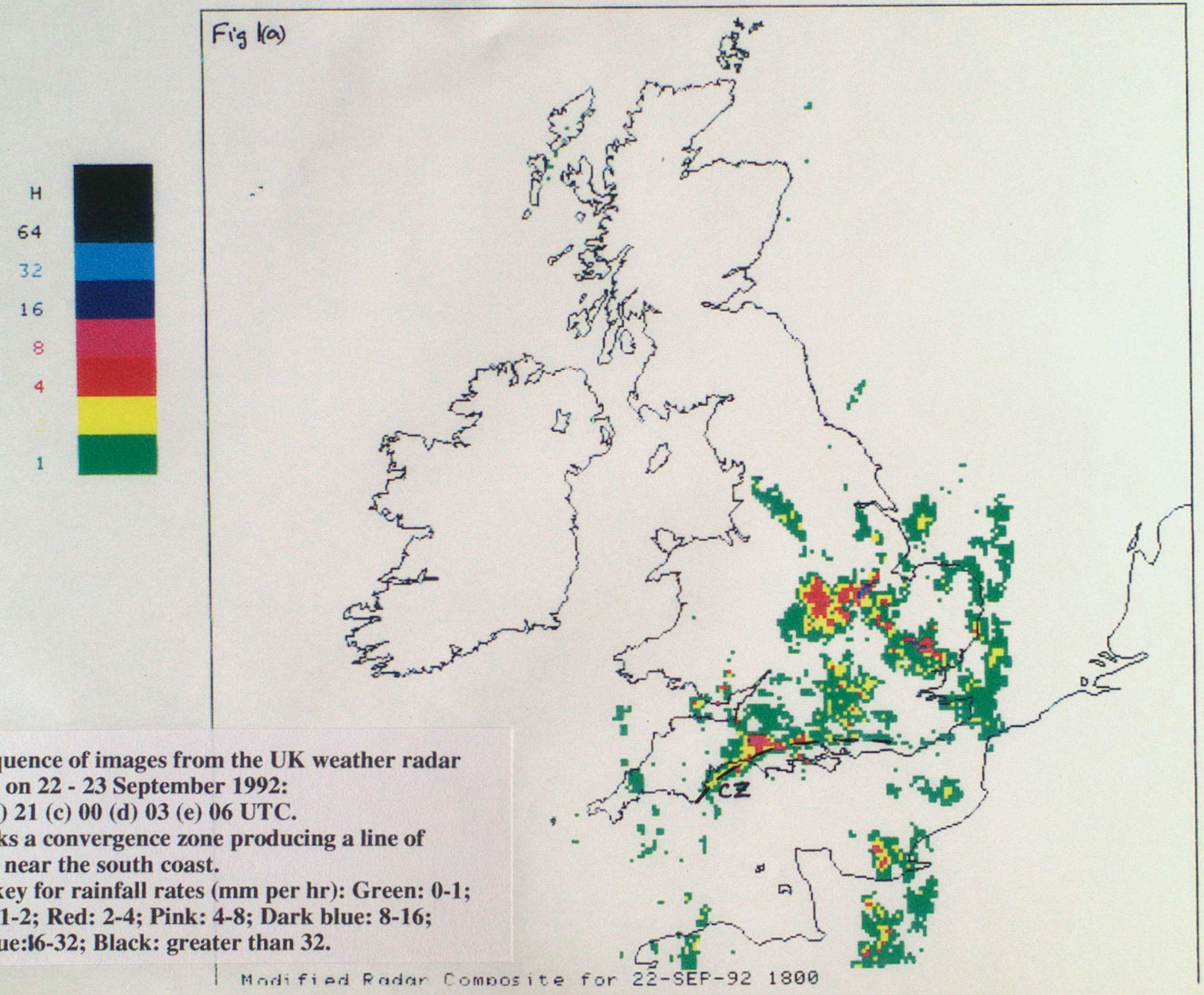

Fig. 1 Sequence of images from the UK weather radar network on 22 - 23 September 1992:
(a) 18 (b) 21 (c) 00 (d) 03 (e) 06 UTC.
CZ marks a convergence zone producing a line of showers near the south coast.
Colour key for rainfall rates (mm per hr): Green: 0-1; Yellow: 1-2; Red: 2-4; Pink: 4-8; Dark blue: 8-16; Light blue: 16-32; Black: greater than 32.

Fig 1 (b)

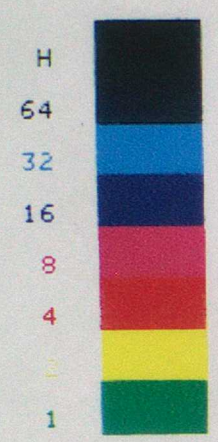

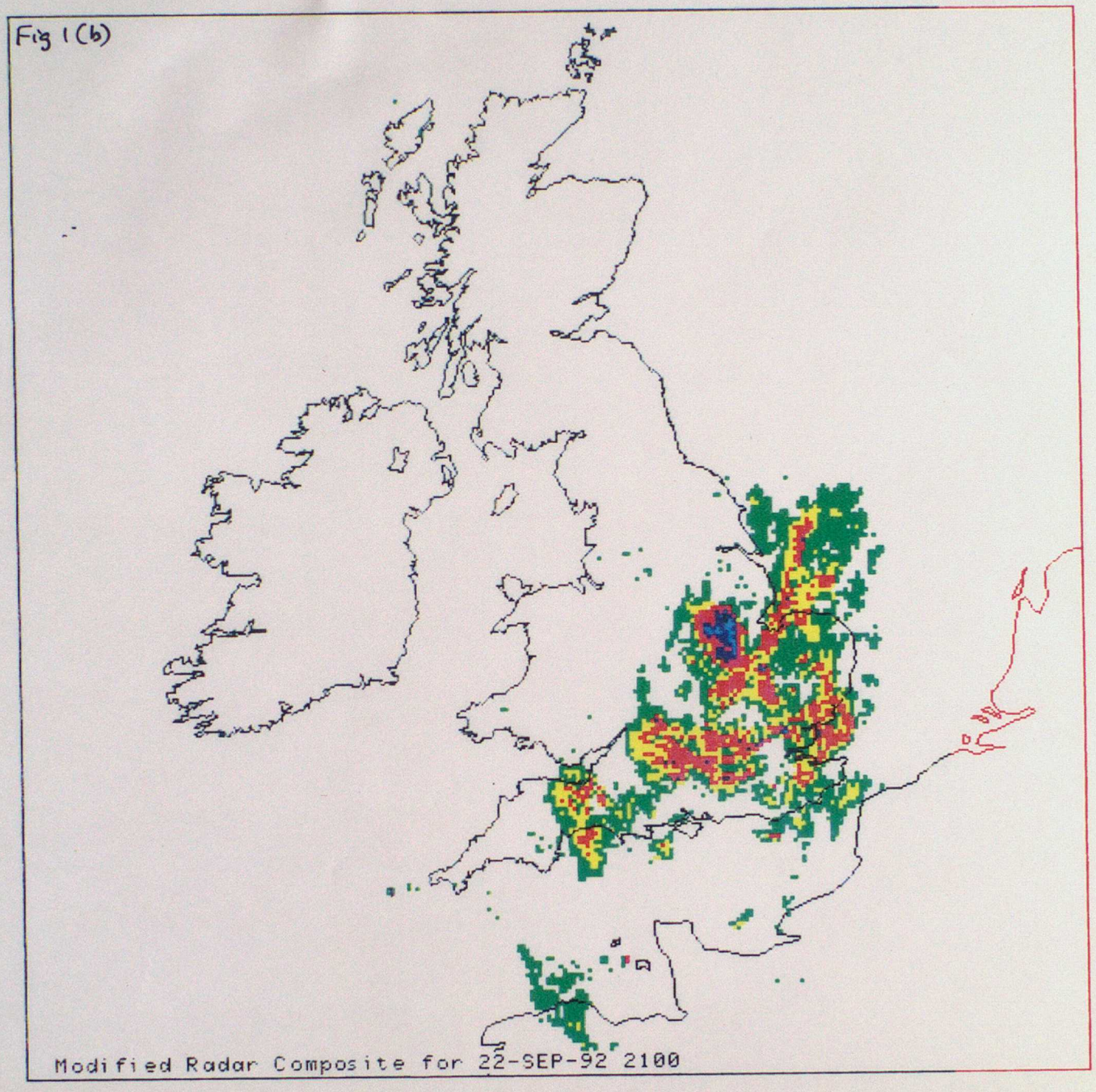

Fig 1(c)

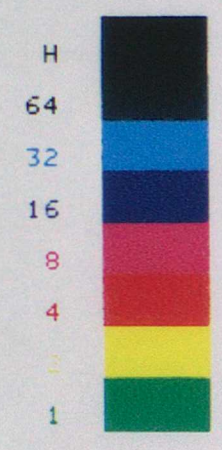

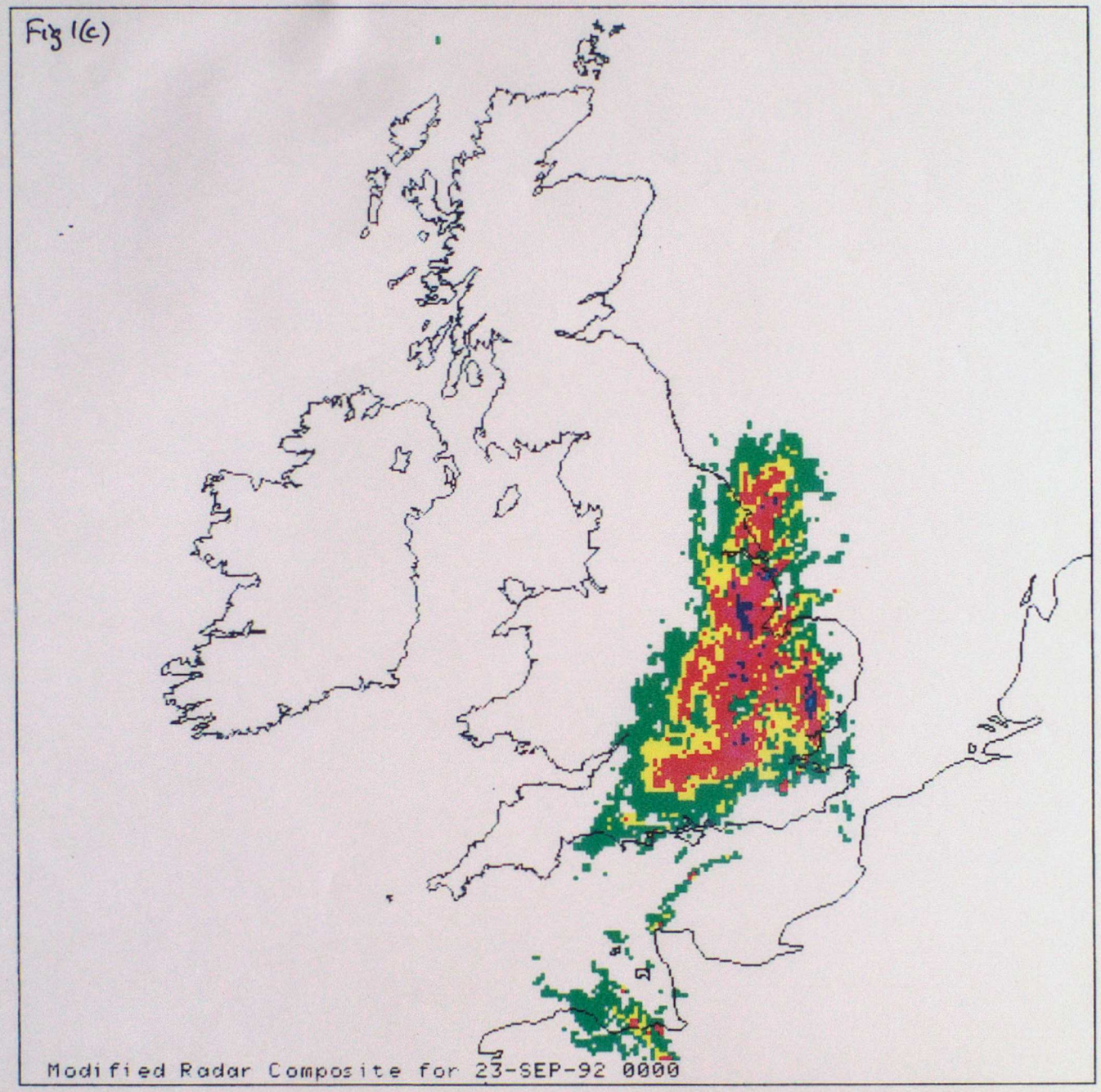

Fig 1(d)

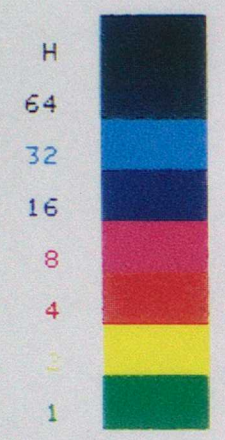

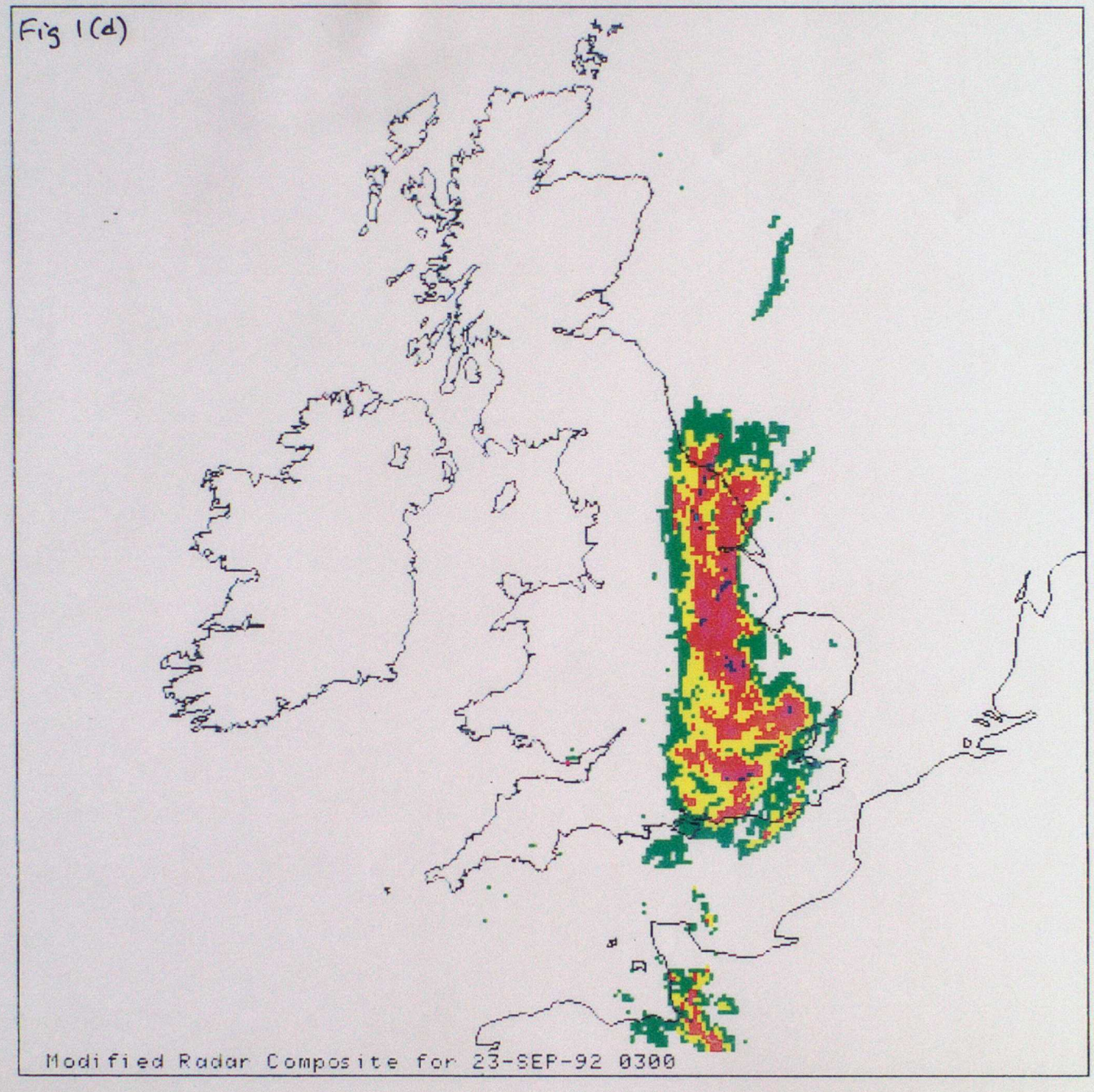

Fig 1(e)

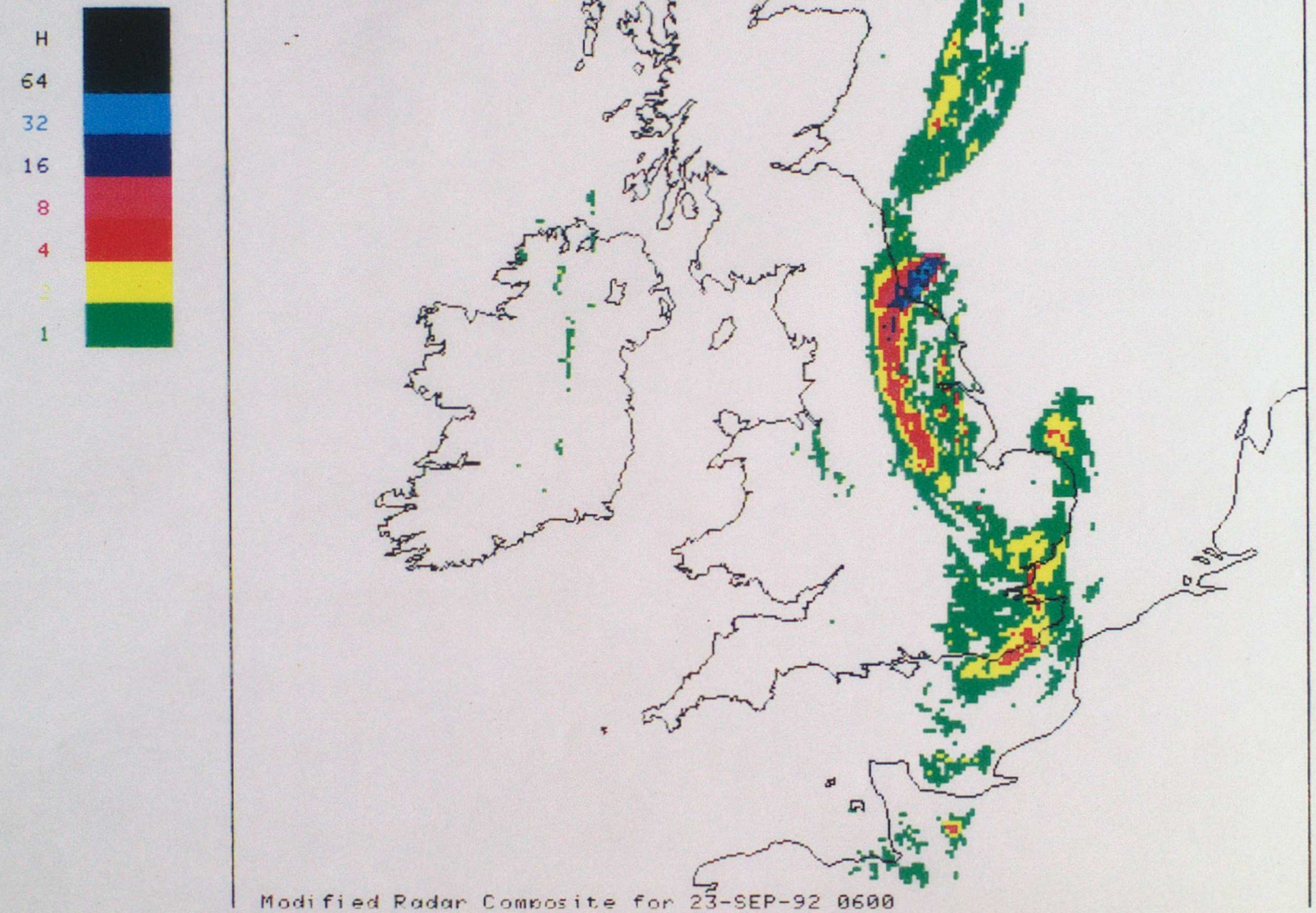

Fig. 2 24-hour rainfall totals (mm) to 09 UTC on 23 September 1992. M shows location of floods illustrated in Fig. 3.

FLOOD CHAOS HITS COUNTY

Man dies as villages and roads suffer

FLOODS wreaked havoc in Leicestershire today. One person died, homes were evacuated, villages cut off and roads blocked after a night of torrential rain.

Large areas of the county were under up to five feet of water. Rivers and streams were close to bursting their banks.

One hundred homes in Barkby had to be evacuated as the waters continued rising this afternoon. Houses in Ashby Folville and Syston were also evacuated.

Trains disrupted and main roads closed

Almost two inches of rain fell overnight the highest 24-hour total on record for September. And weather experts warned there was more to come.

Emergency services said they were at full stretch dealing with a string of incidents.

Leicestershire police scrambled their helicopter in a bid to pinpoint problems.

Chaos was brought to the morning rush-hour, with train services severely disrupted, vehicles stranded and main roads closed.

Watermead Way, in Leicester, was blocked when a man died in an accident involving a lorry at around 6am.

Another driver was taken to hospital following a four-vehicle pile-up which blocked two out of three lanes on the A47 near East Norton.

Villagers in the east and south of the county woke up to find roads turned into rivers.

Brookfield Street, in Syston, Crow Mills, in South Wigston, and the villages of Walcote, near Lutterworth, and Ashby Folville, near Melton, were among the worst affected areas. The village pub at Ashby Folville became a refuge for 10 people who had to leave their flooded homes.

A brook burst its bank, sending water swirling through the village which was entirely cut off.

Fire crews, police and local farmers with tractors, trailers and Land Rovers helped in the evacuation operation.

Those rescued were taken to the Carrington Arms, where licensee Mr Mick Farmer and his wife

■ Continued, Page 3

by Staff Reporters

LEADING HORSE THROUGH WATER: The scene at the Carrington Arms, Ashby Folville, near Melton, today, where villagers took refuge from the floodwaters

FLOODED ROADS TO AVOID

POLICE report the following roads impassable:
Tur Langton to Cranoe road; Dingley Lane, Market Harborough; Numerous side roads off A427 between Lutterworth and Market Harborough; Farndon Road, Coventry Road End; Brook Street, Walcote; Laughton and Lubbenham road; Bruntingthorpe Road junction, Peatling Parva/Magna junction; Walcote and Kimcote road; Beeby; Hamilton Lane; Beeby to Hungarton; Barkby village to Humberside Lane; Melton Road, Thurmaston — impassable city-bound at Roundhill College; High Street, Syston — impassable under railway bridge.
Passable with care: Cricketers Hill, Barkby Thorpe; Fillingate Road, Wanlip Road, Wanlip; Wanlip Lane, Syston, near Hope and Anchor; Hungarton Lane and Main Street, Beeby; Queniborough Road, South Croxton;
A427 Husbands Bosworth side of Theddingworth between Ashby Magna and Willoughby Waterleys; Gilmorton Road, one mile outside Lutterworth; Cromwell Crescent, Market Harborough.
Barely passable: Grange Lane, Thurnby.

Fig. 3 Front page of the Leicester Mercury on 23 September 1992.

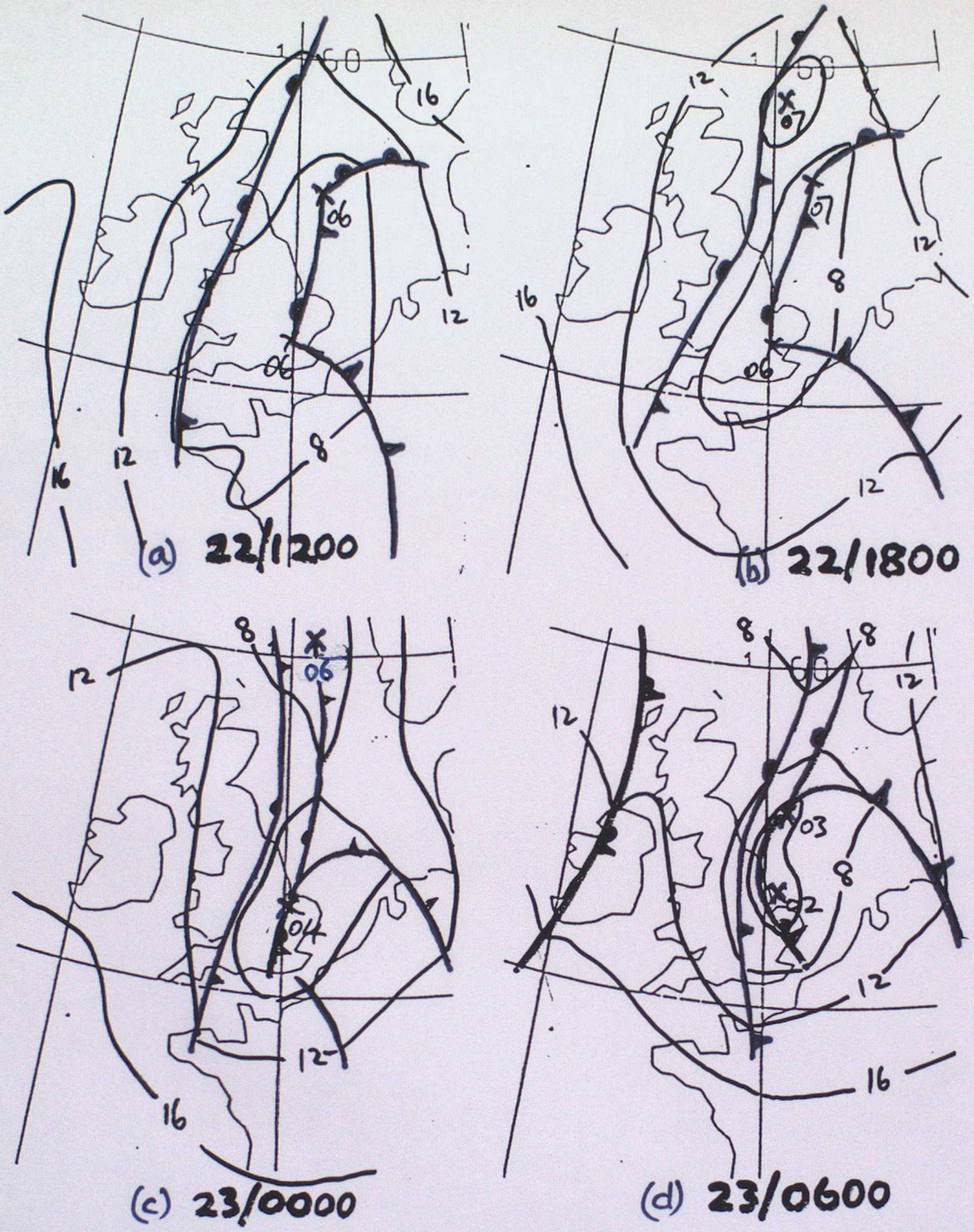

Fig. 4 Surface analyses at 6 hourly intervals on 22 - 23 September 1992.
(a) 12 (b) 18 (c) 00 (d) 06 UTC.

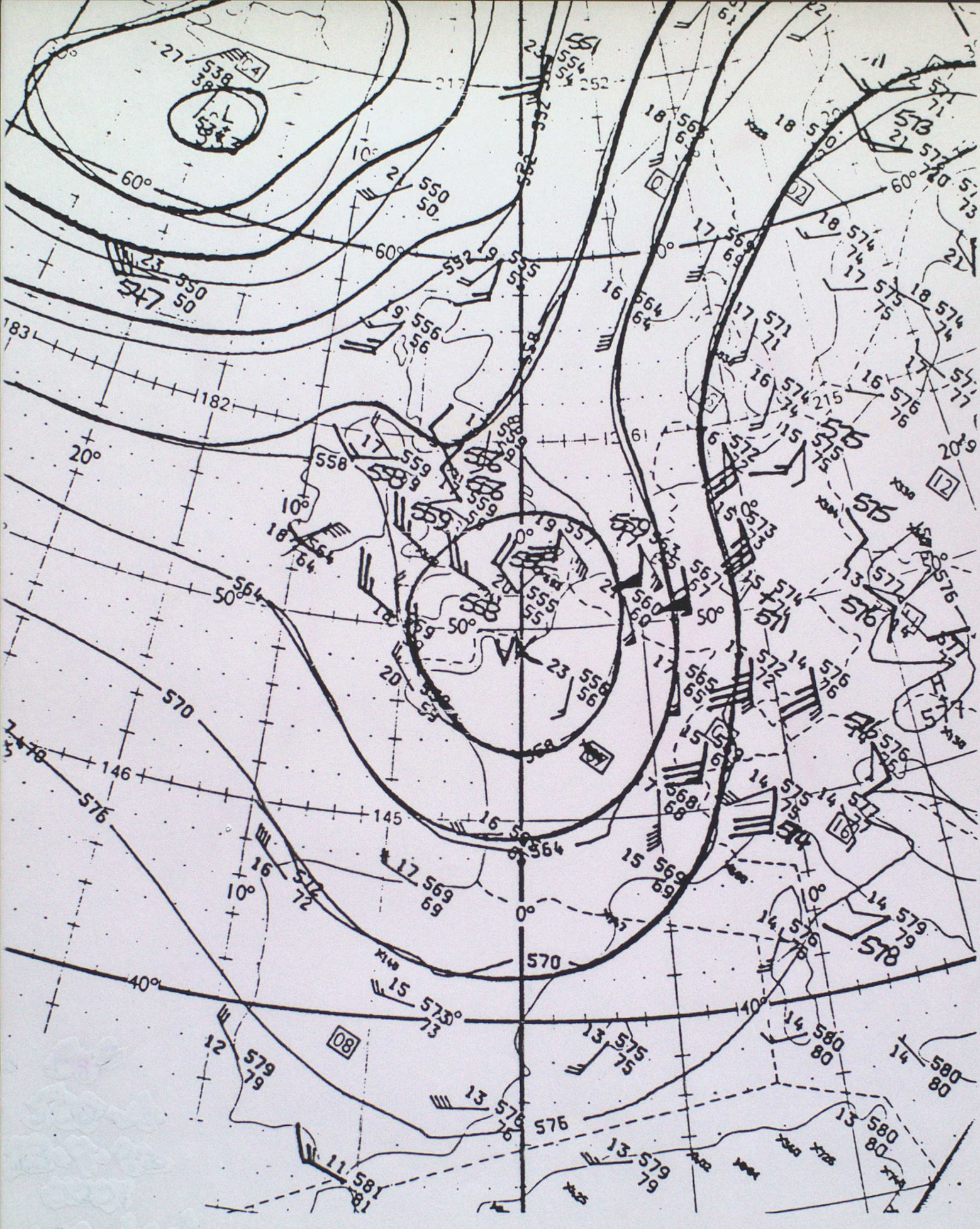

Fig. 5 CFO working chart of 500 hPa contours (dam) and winds (knots) at 00 UTC on 23 September 1992. Certain stations have winds at 06 UTC overplotted.

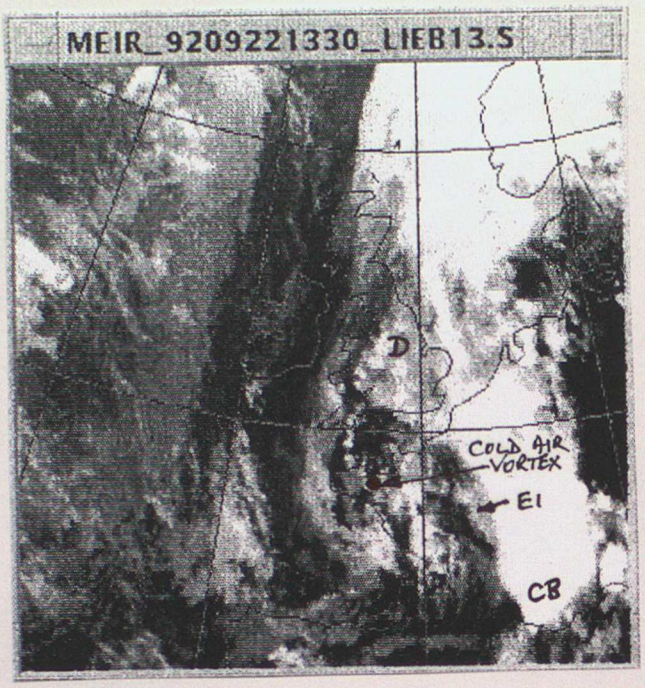

6 (a)

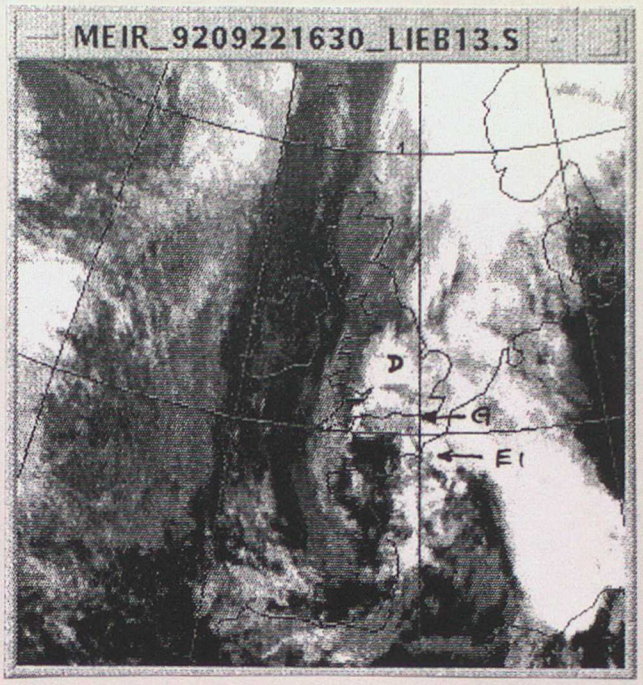

6 (b)

6 (c)

6 (d)

Fig. 6 METEOSAT images on 22 September 1992:
(a) IR at 1330 UTC,
(b) IR at 1630 UTC,
(c) IR at 1830 UTC,
(d) IR at 2230 UTC,
(e) WV at 21 UTC.

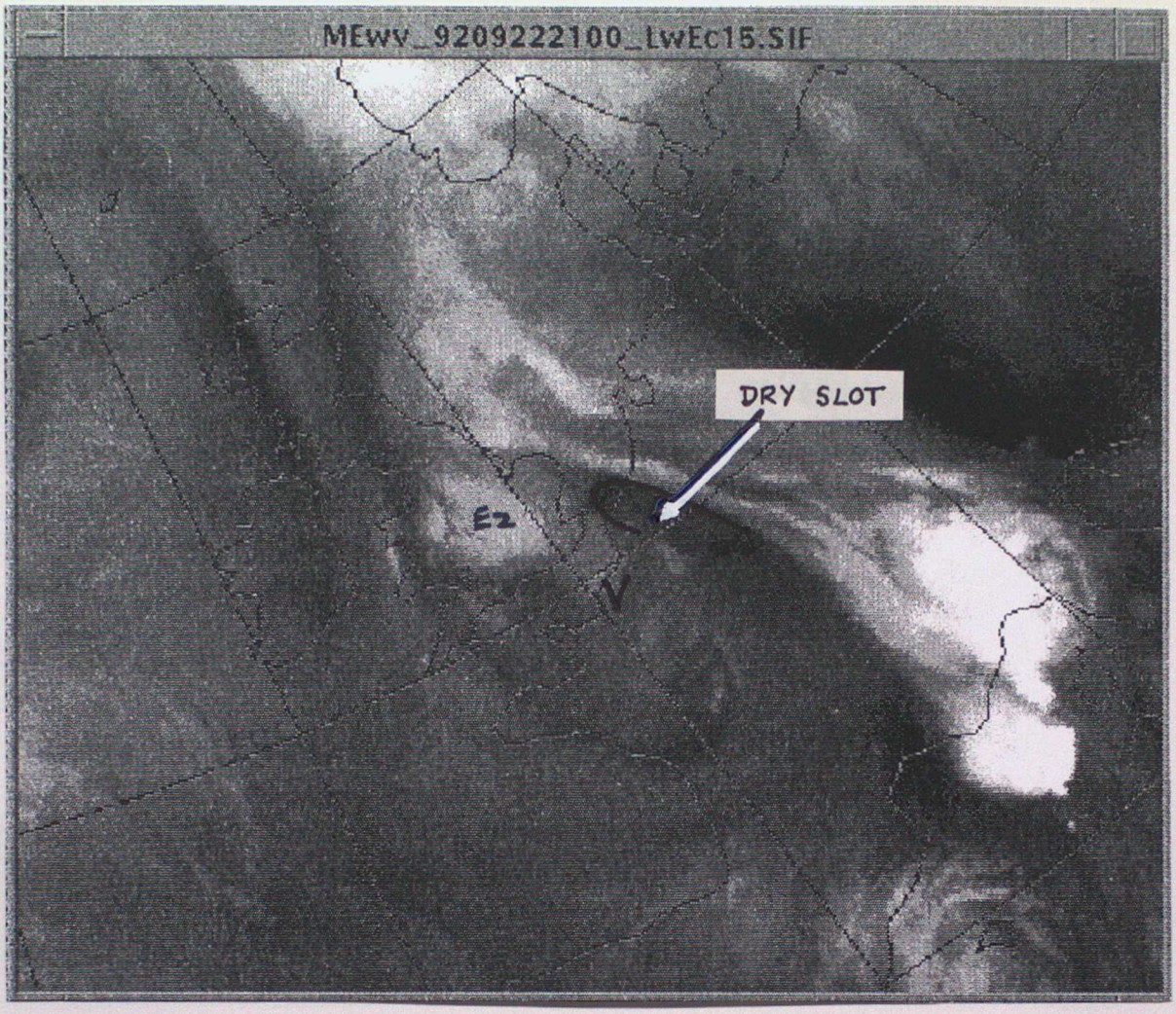

6(e)

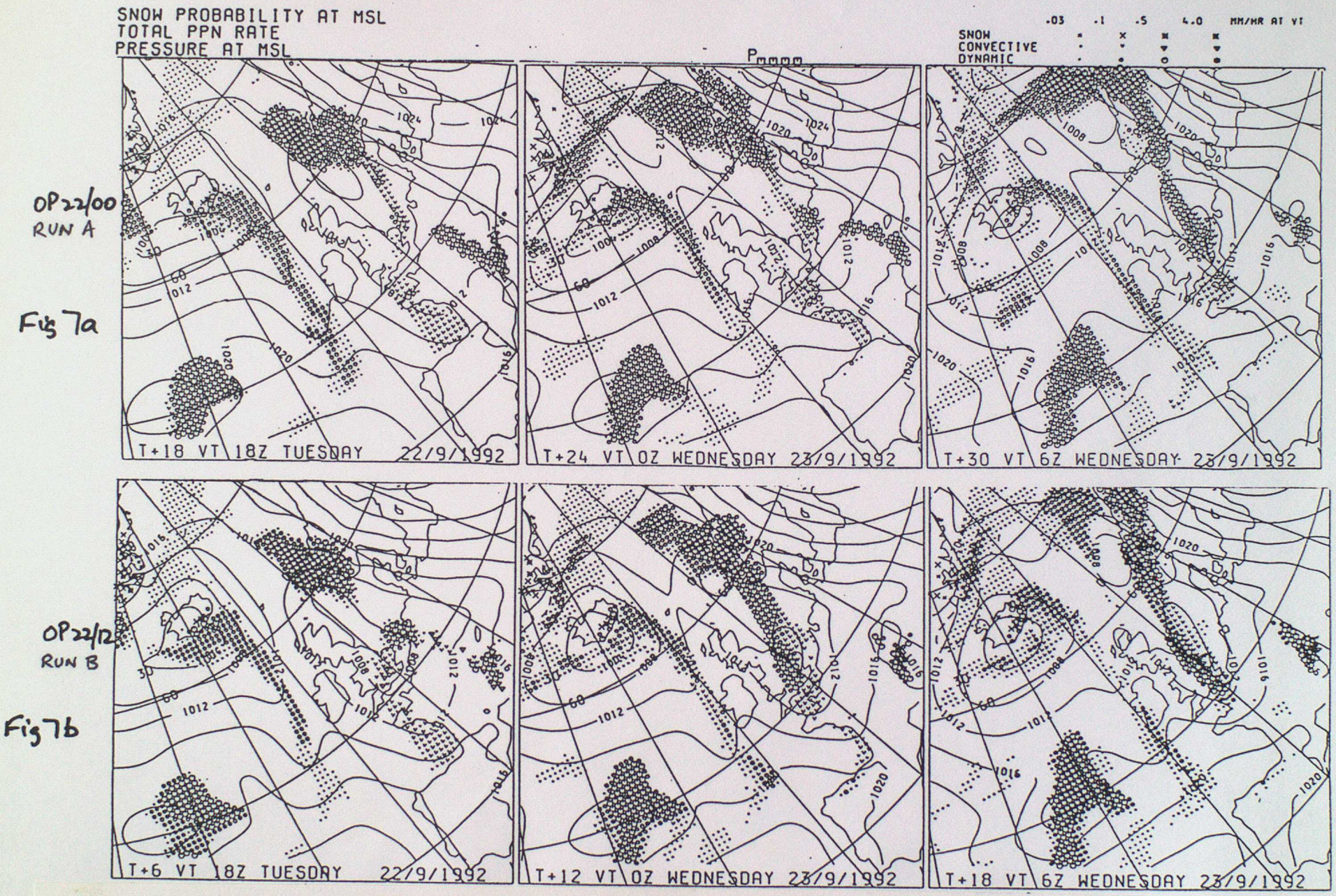

Fig. 7 Forecasts of MSLP (isobars, hPa) and rainfall rate (mm hr^{-1}) at 18, 00 and 06 UTC on 22 - 23 September 1992 from the LAM run at:
(a) 00 UTC on 22nd (Run A), (b) 12 UTC on 22nd (Run B).

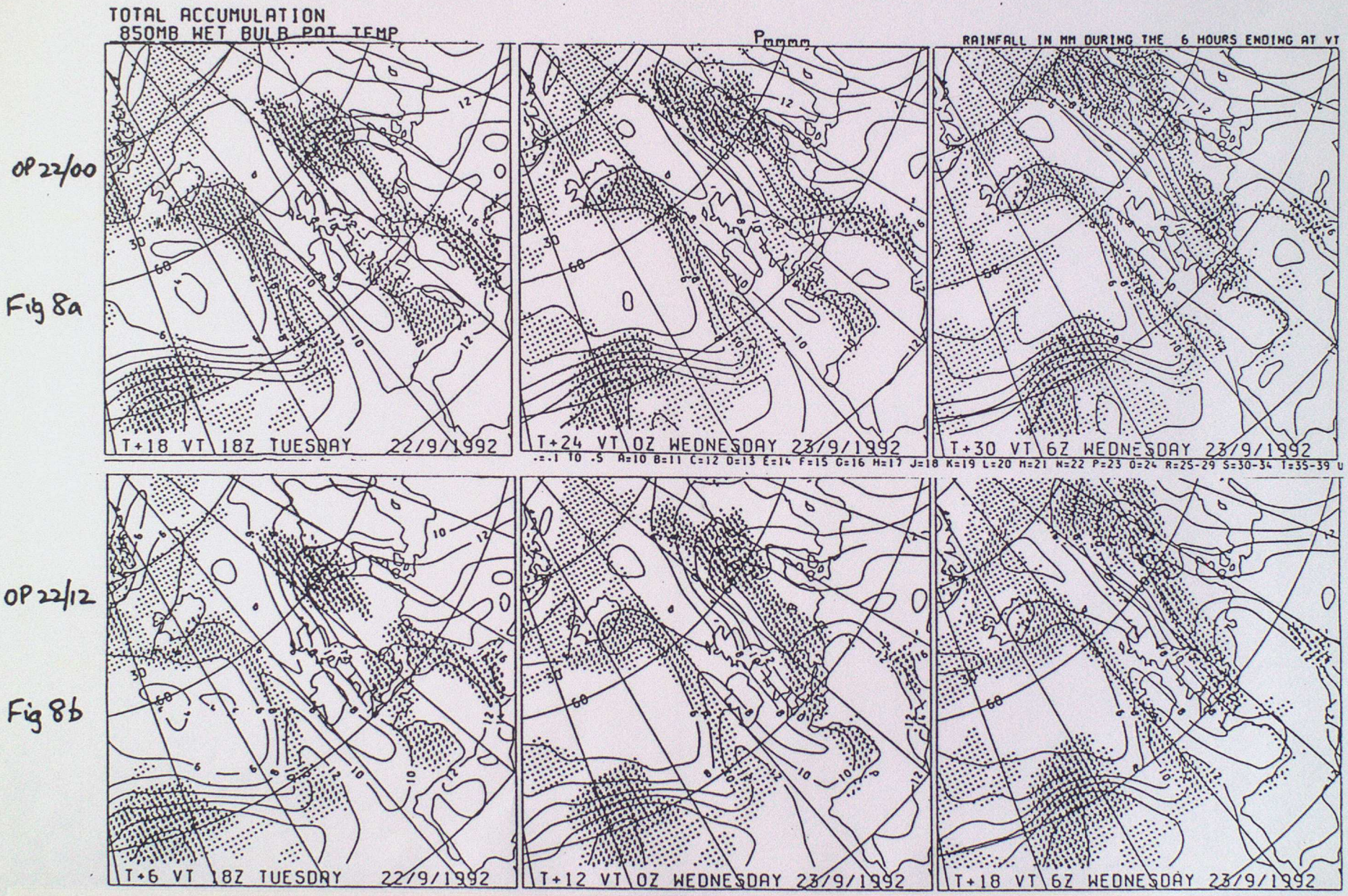

OP 22/00

Fig 8a

OP 22/12

Fig 8b

Fig. 8 Forecasts from the LAM of 850 hPa wet-bulb potential temperature (WBPT, isotherms, deg. C)) and 6-hourly rainfall accumulations (mm) for the same verifying times and runs as Fig. 7.

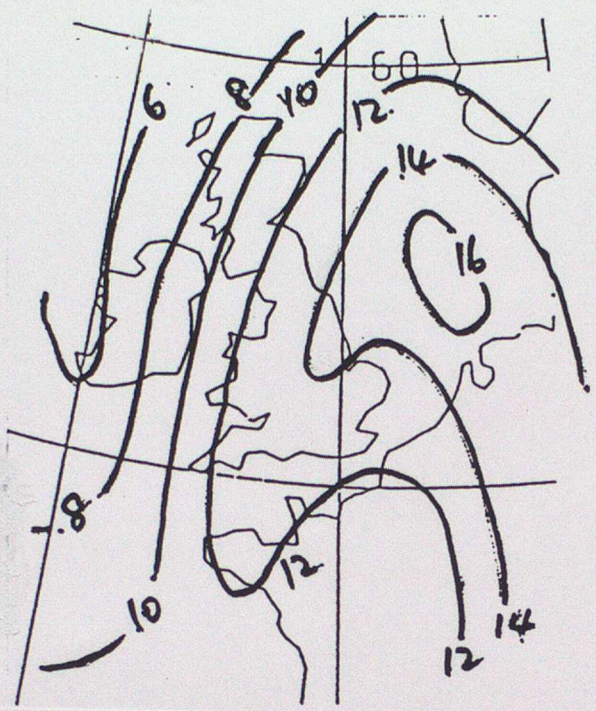

Fig. 9 WBPT (deg. C) at 850 hPa at 12 UTC on 22nd September analysed from radiosonde reports.

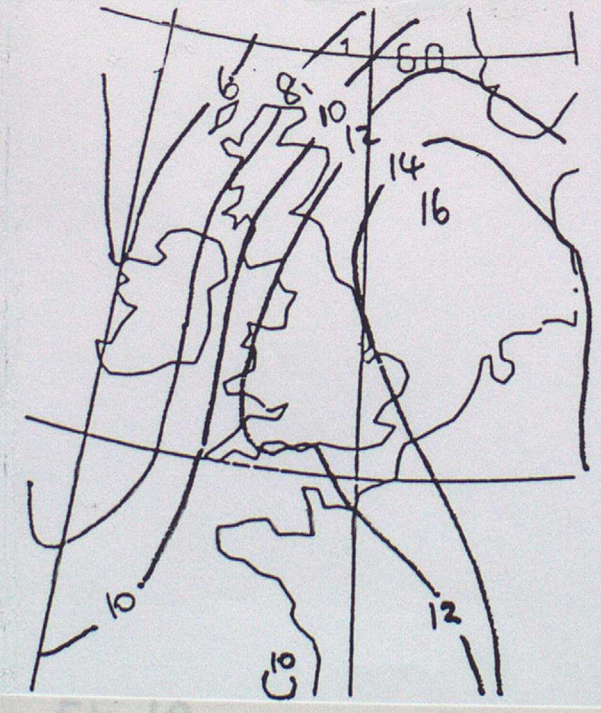

Fig. 10 Forecast of WBPT (deg. C) at 850 hPa for the same time as Fig. 9 from Run A.

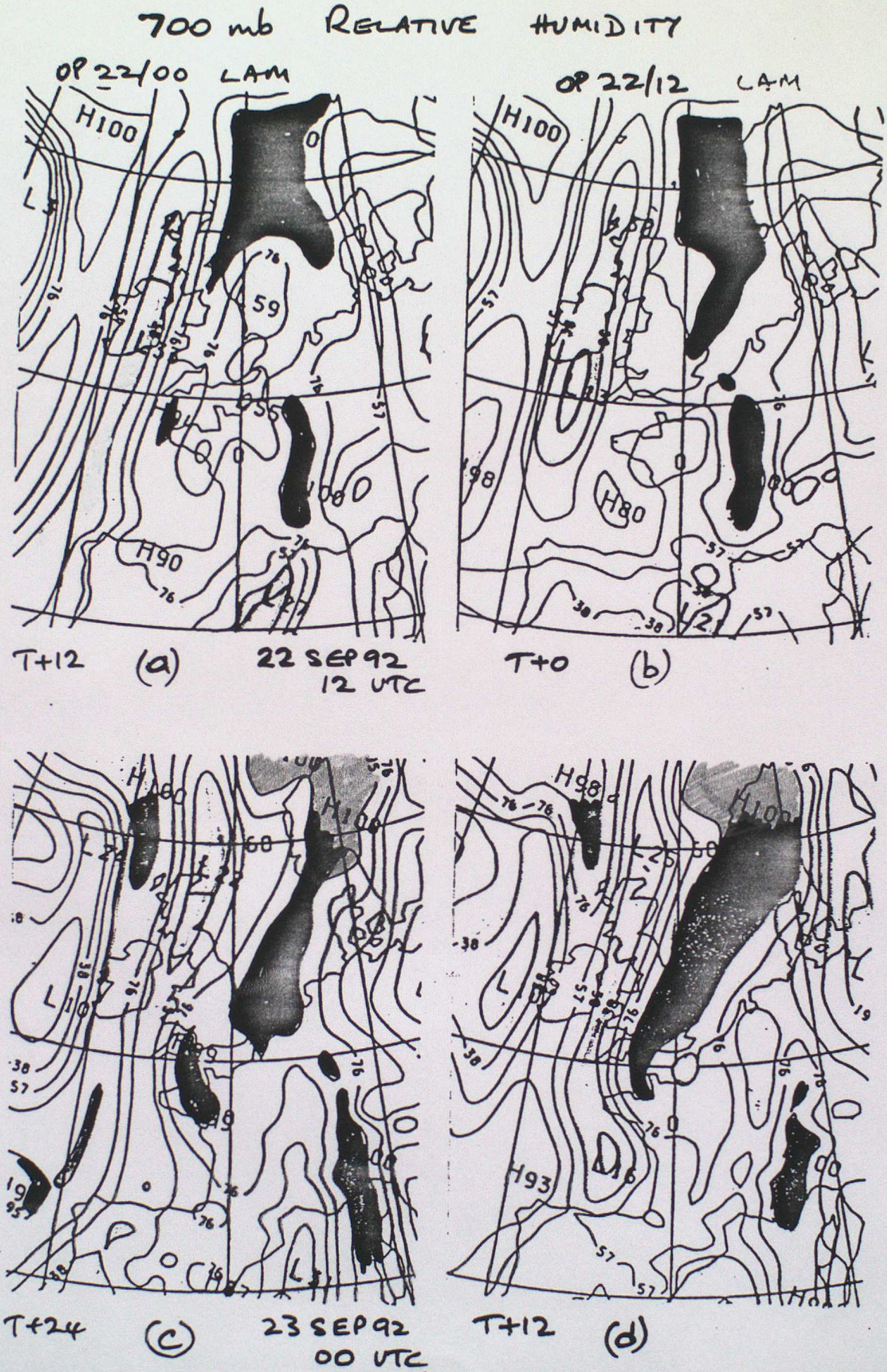

Fig. 11 Model relative humidity (%) at 700 hPa for
(a) 12 UTC on 22nd from Run A of the LAM (i.e. 12 hour forecast)
(b) 12 UTC on 22nd from Run B (i.e. analysis)
(c) 00 UTC on 23rd from Run A (i.e. 24 hour forecast)
(d) 00 UTC on 23rd from Run B (i.e. 12 hour forecast)
Areas with relative humidity greater than 95 % are shaded.

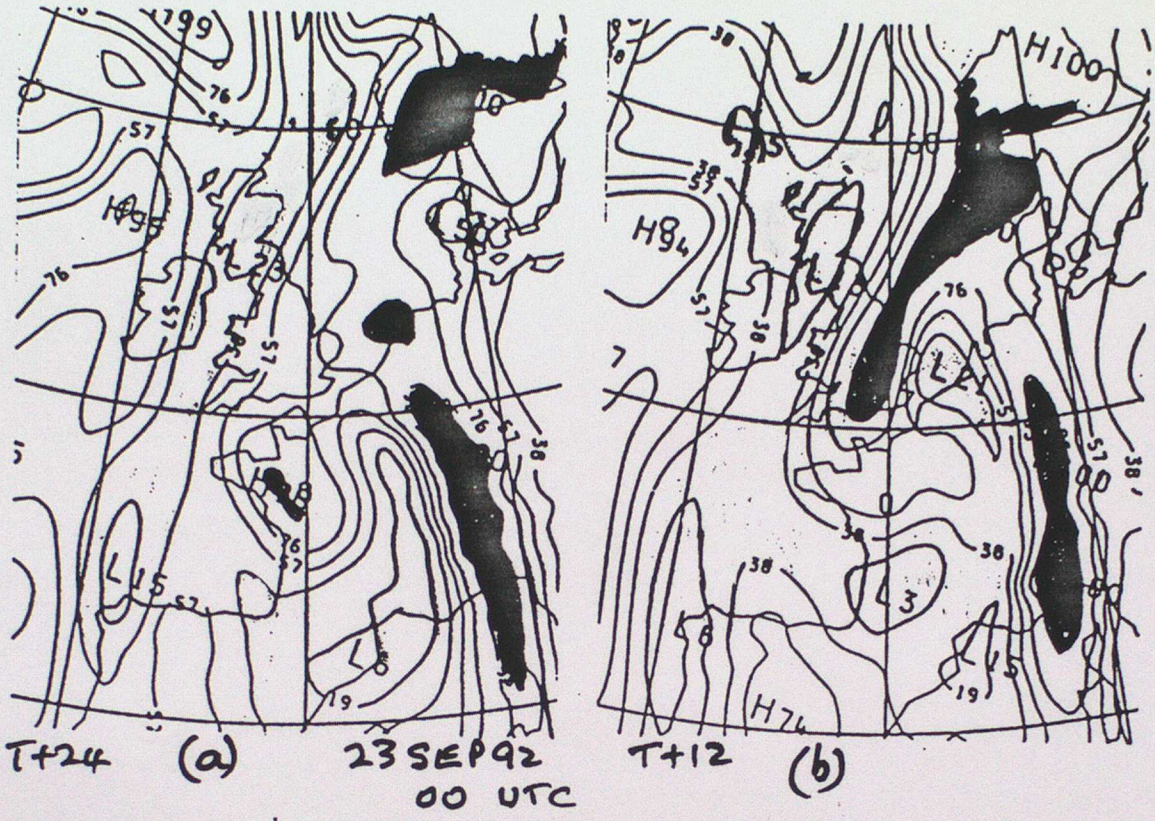

Fig. 12 Relative humidity (%) at 500 hPa for 00 UTC on 23rd September
(a) from Run A of the LAM (i.e. 24 hour forecast)
(b) from Run B (i.e. 12 hour forecast)

Areas with relative humidity greater than 95 % are shaded.

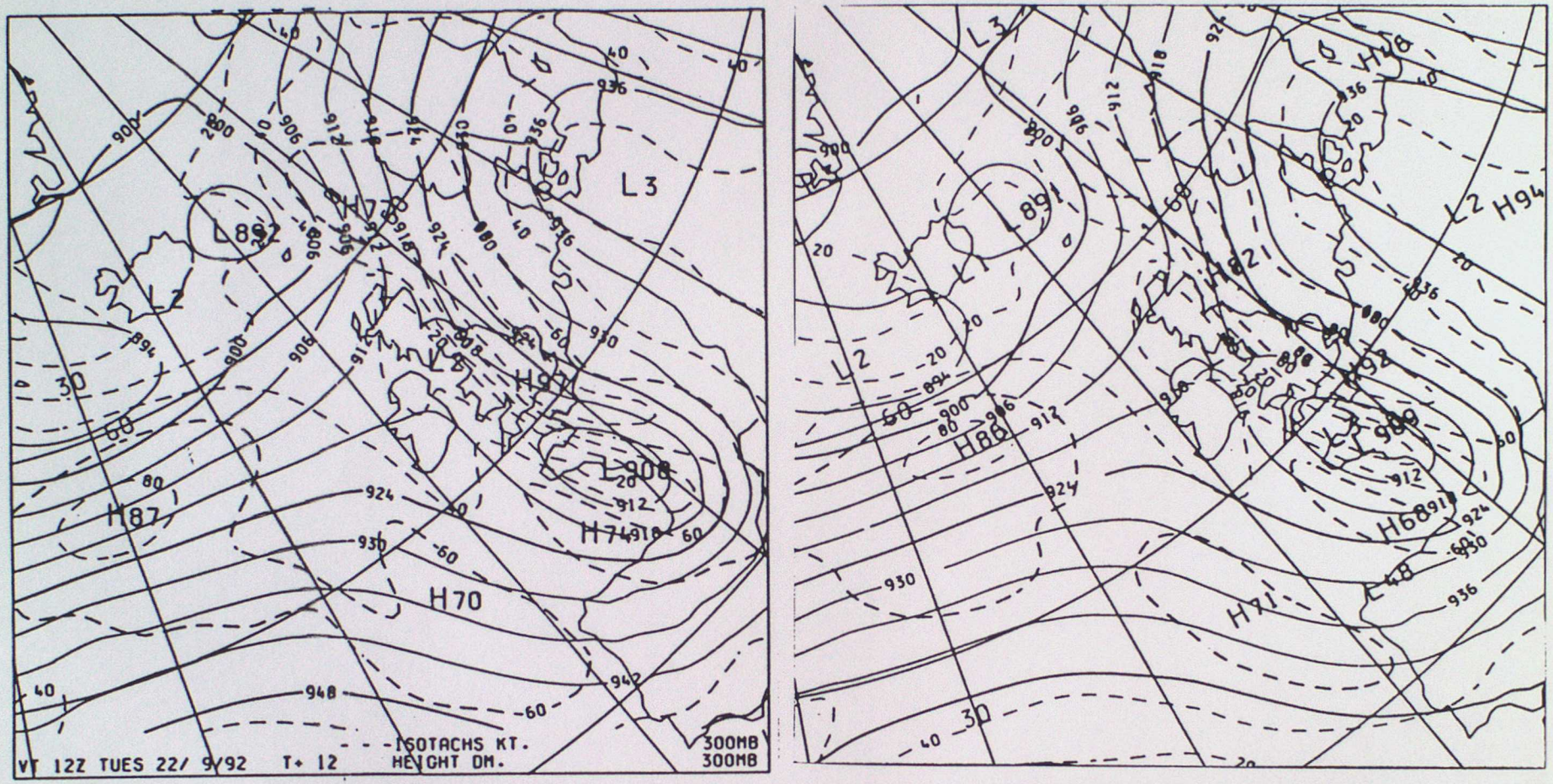

Fig. 13 300 hPa height (continuous lines, dam) and isotachs (dashed lines, knots) at 12 UTC on 22nd September from (a) Run A (i.e. 12 hour forecast), (b) Run B (i.e. analysis).

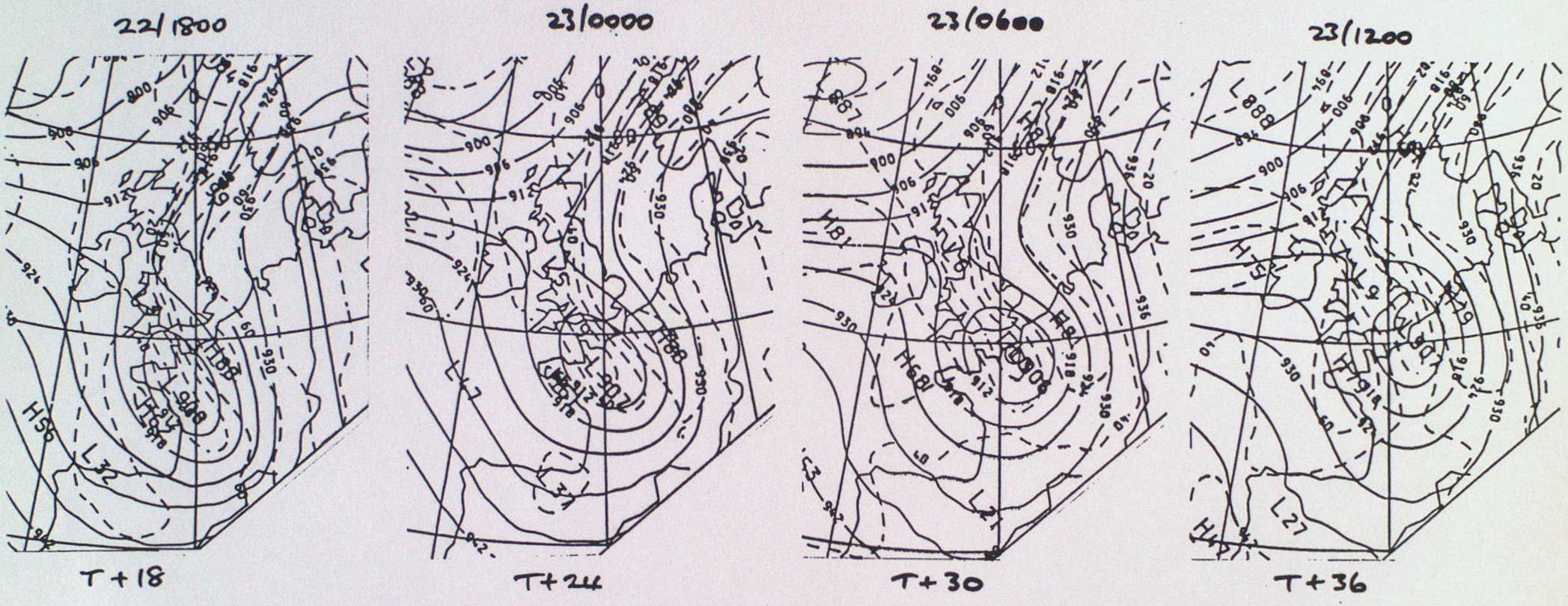

Fig. 14 LAM forecasts of 300 hPa height (continuous lines, dam) and isotachs (dashed lines, knots) from (a) Run A and (b) Run B. Times are indicated. P and U in (b) show locations of Paris and Uccle.

LAM 22.9.92 1200 RUN

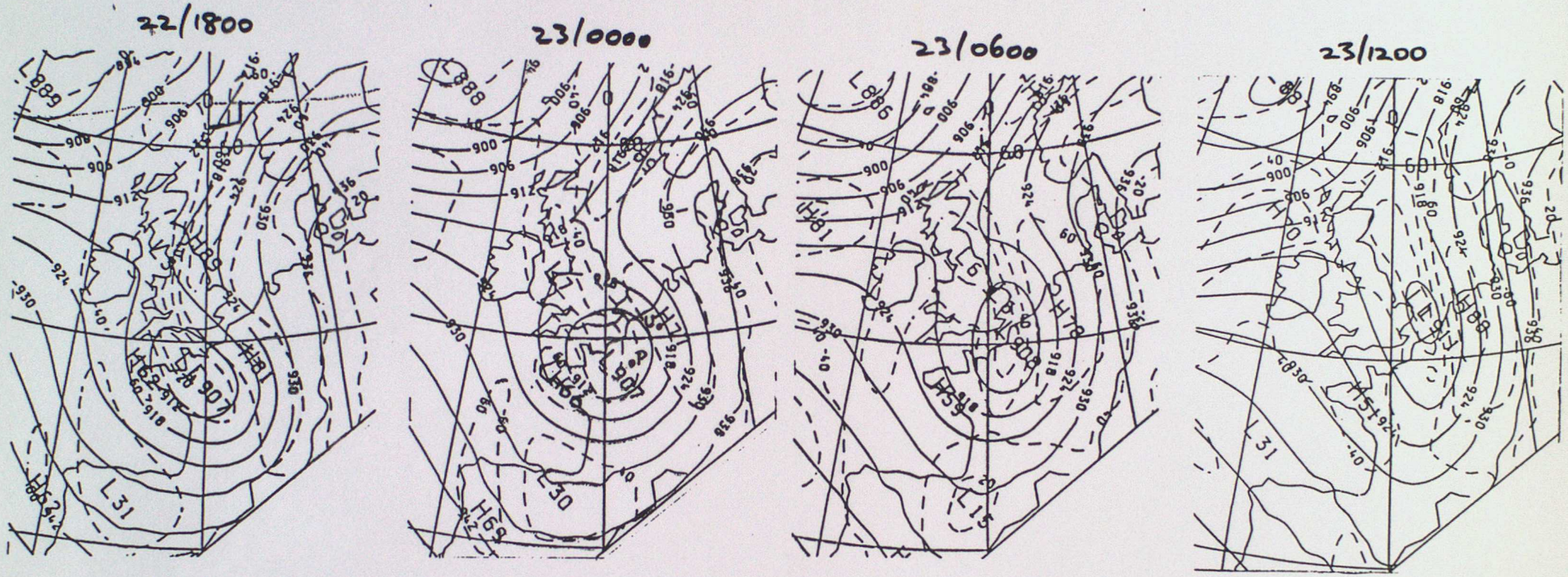

Fig 14b RUN B

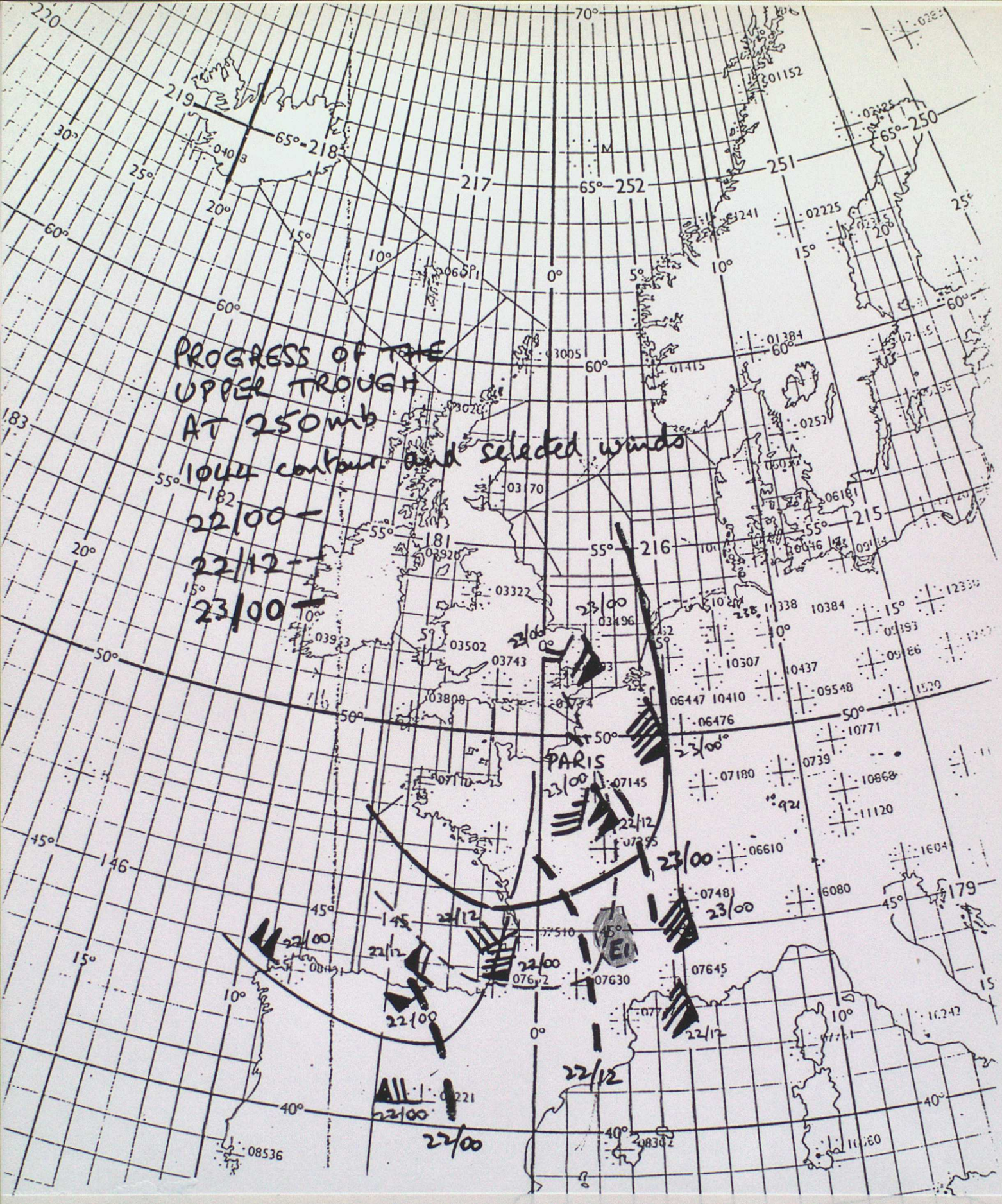

Fig. 15 Observed winds at 250 hPa. Times are indicated on the wind barbs. Dashed lines show the location of a wind veer on an upper level trough which could be followed over Iberia and France during the 22nd September. The shaded area shows the position of cloud area E1 from the satellite image at 1200 UTC.

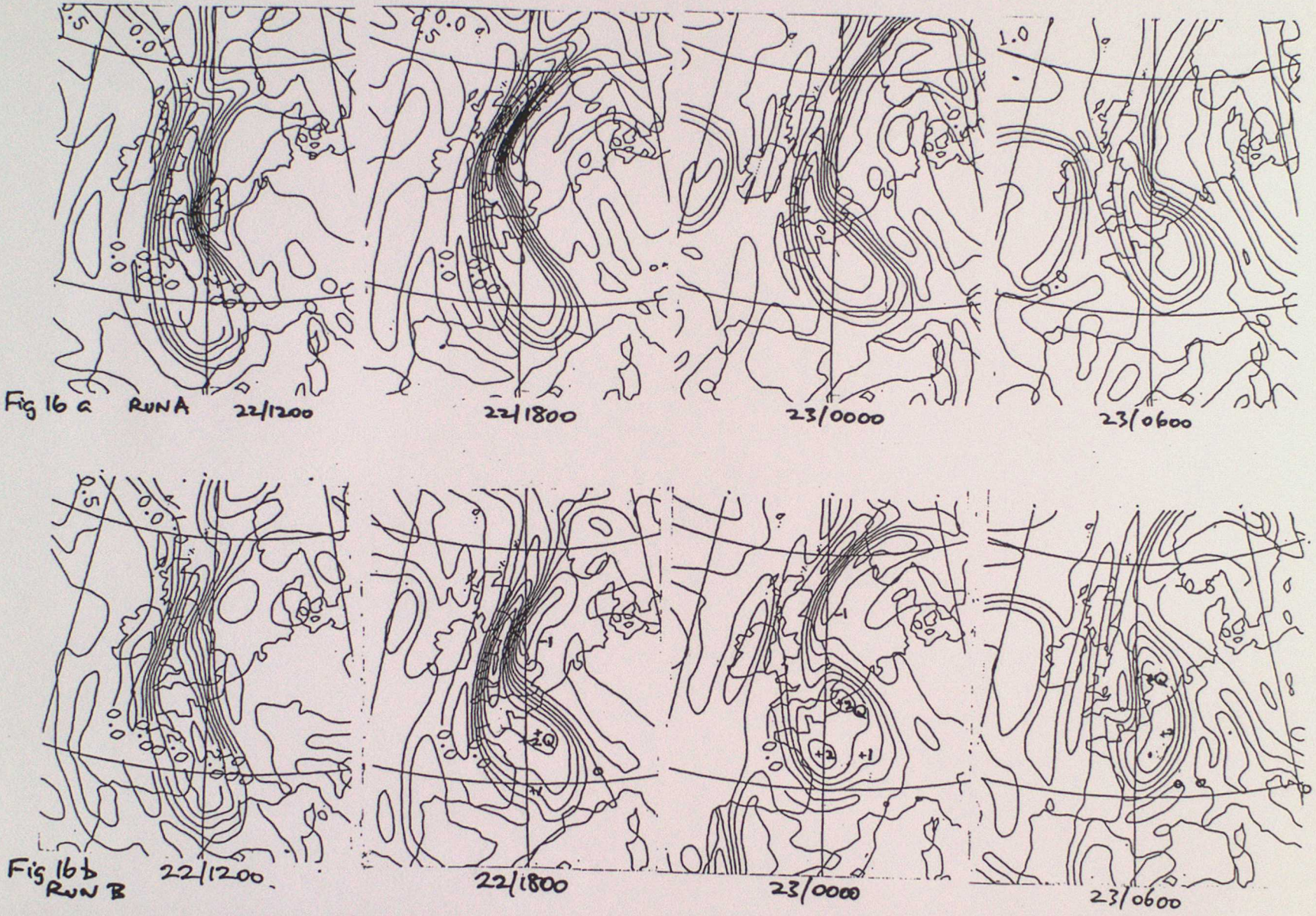

Fig. 16 Vorticity (10^{-4} sec $^{-1}$) at 300 hPa from (a) Run A and (b) Run B at times shown. Q in (b) is a vorticity centre.

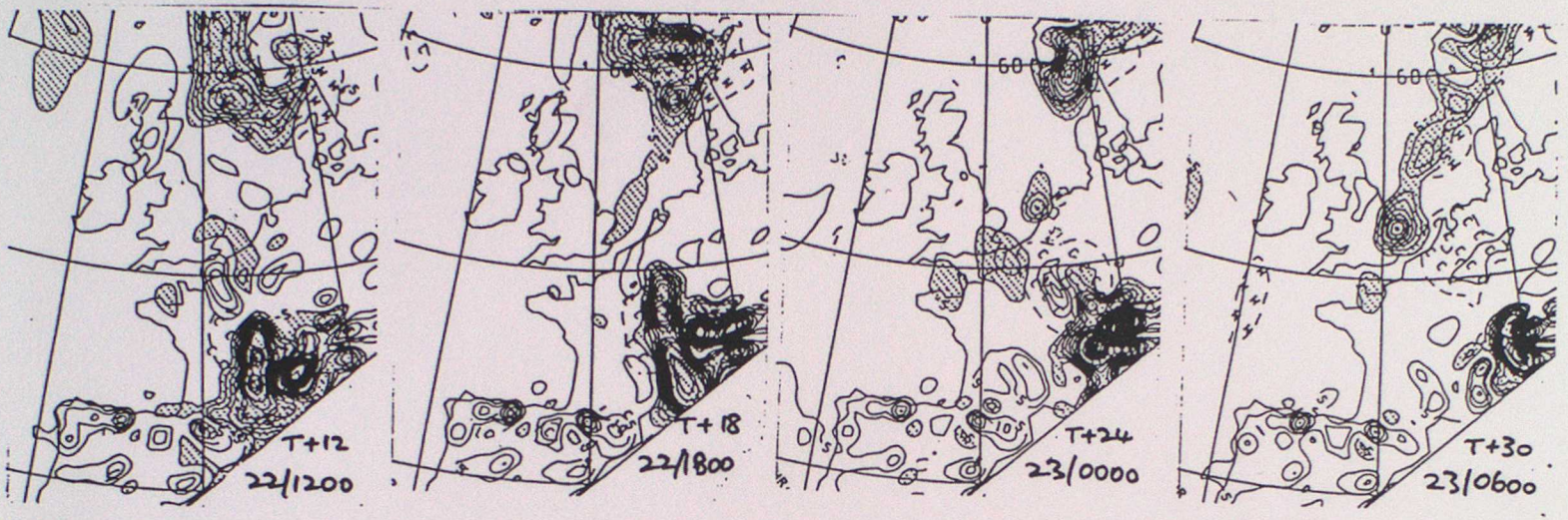

Fig 17a RUN A

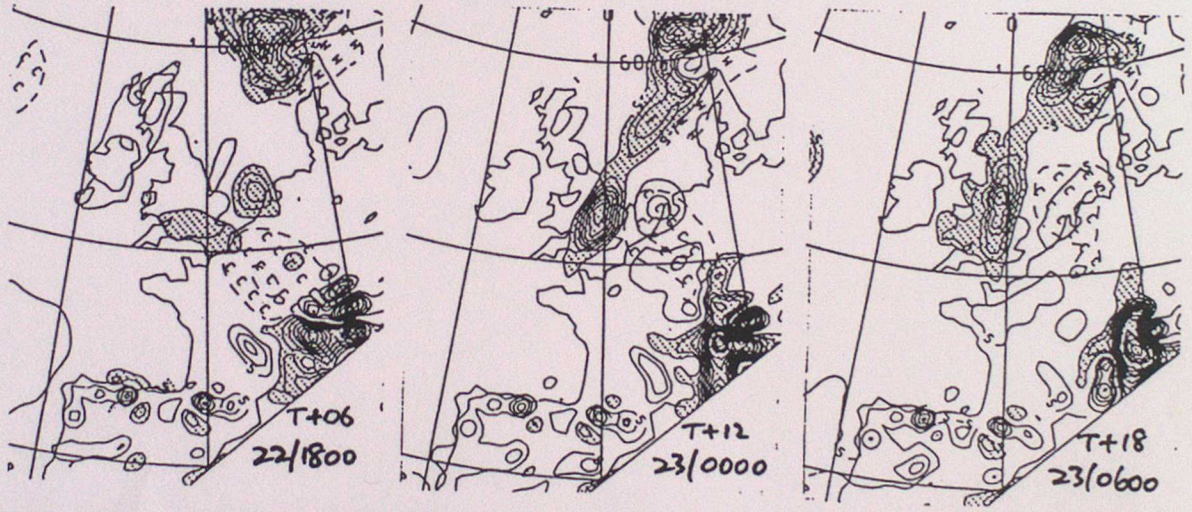

Fig 17b RUN B

Fig. 17 LAM forecasts of vertical velocity (interval of 5hPa hr^{-1}) at 700 hPa (a) from Run A, (b) from Run B at times shown. Stippling shows ascending air.

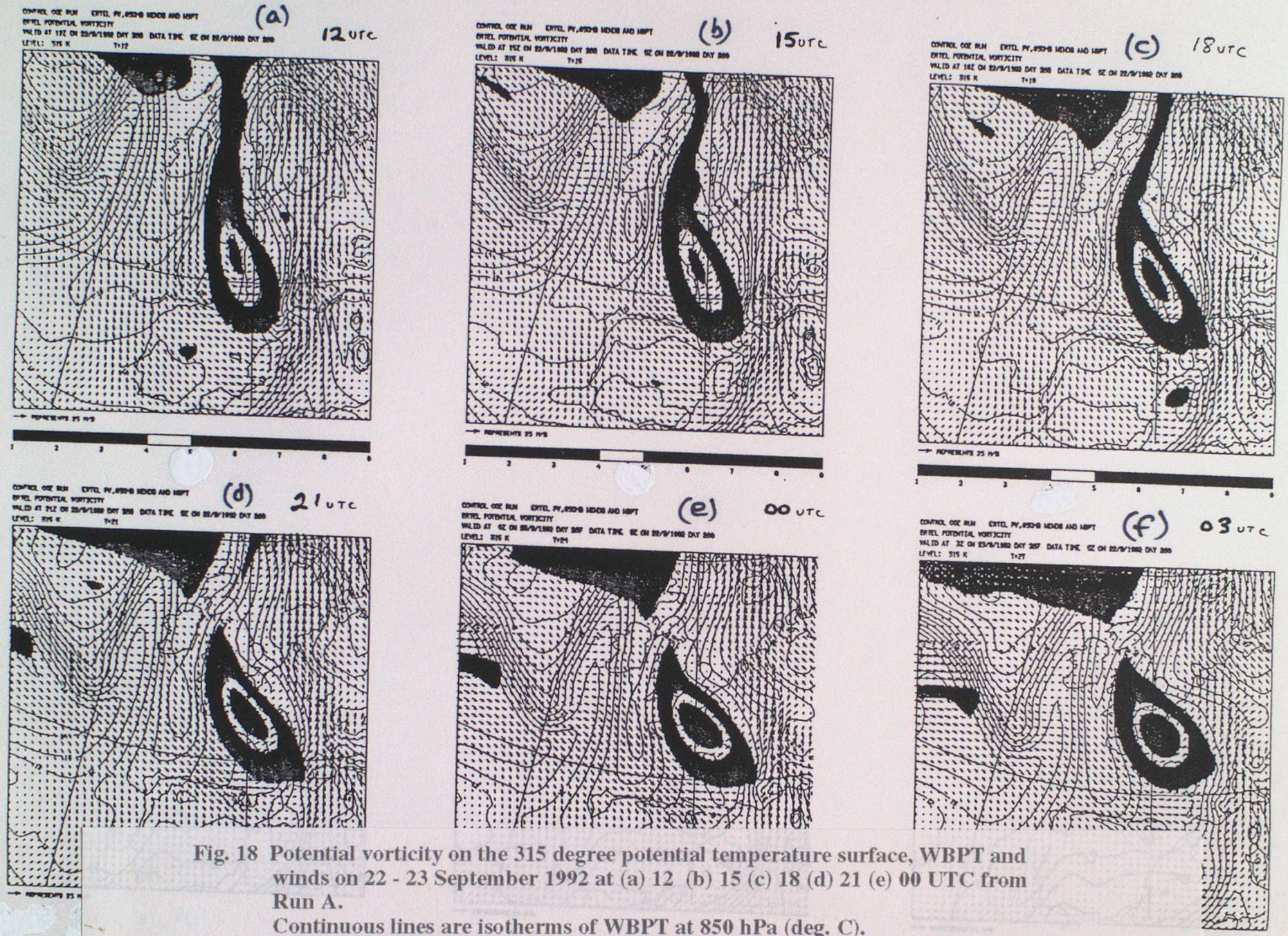

Fig. 18 Potential vorticity on the 315 degree potential temperature surface, WBPT and winds on 22 - 23 September 1992 at (a) 12 (b) 15 (c) 18 (d) 21 (e) 00 UTC from Run A.
Continuous lines are isotherms of WBPT at 850 hPa (deg. C).
Arrows are winds at 850 hPa (metres per sec).
Patterns in white and black show a potential vorticity anomaly at intervals of 2 PV units. Within the black area in the middle of the anomaly, PV exceeds 5 units.

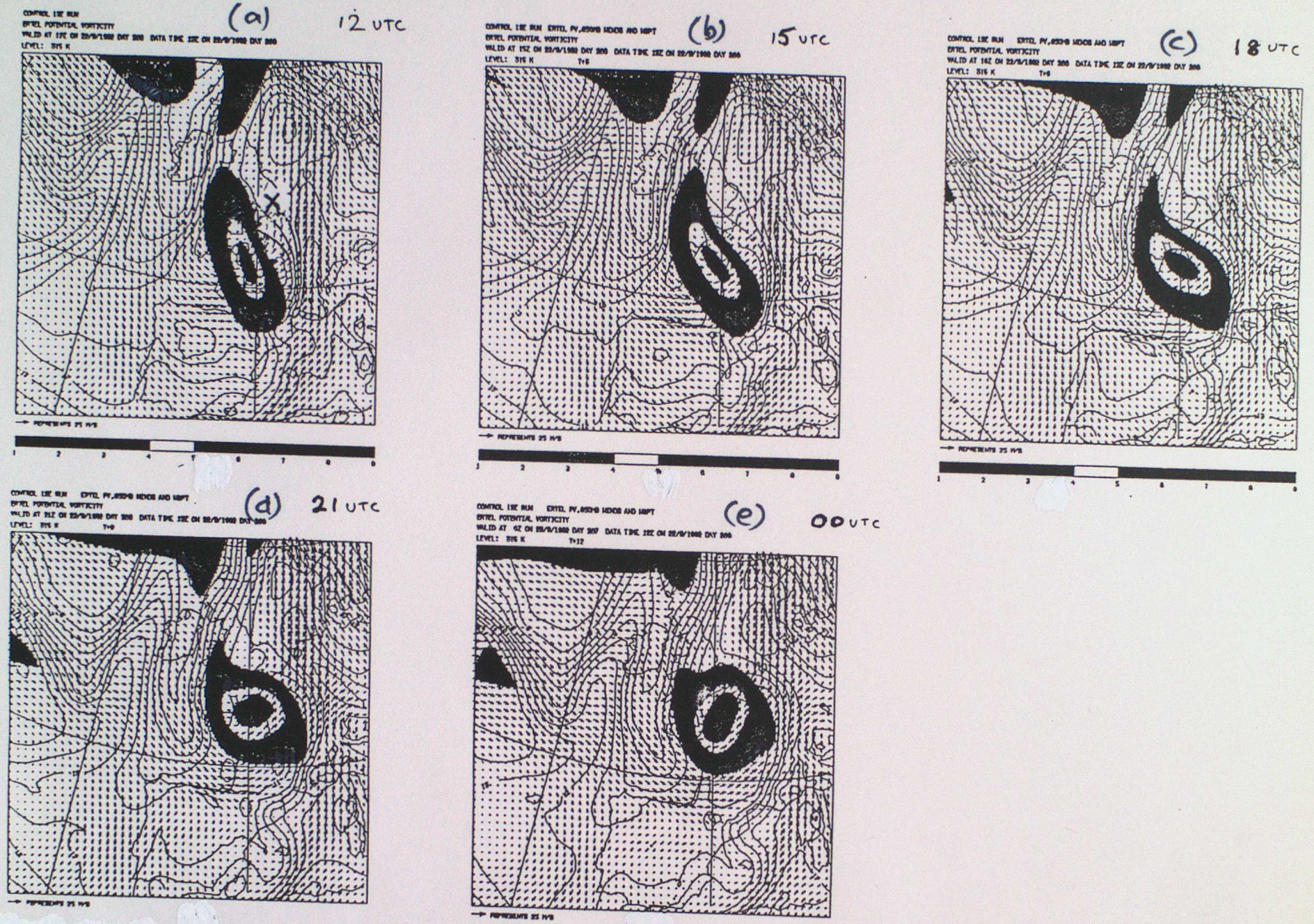

Fig. 19 As Fig. 18, but from Run B. Position X in (a) is explained in the text.

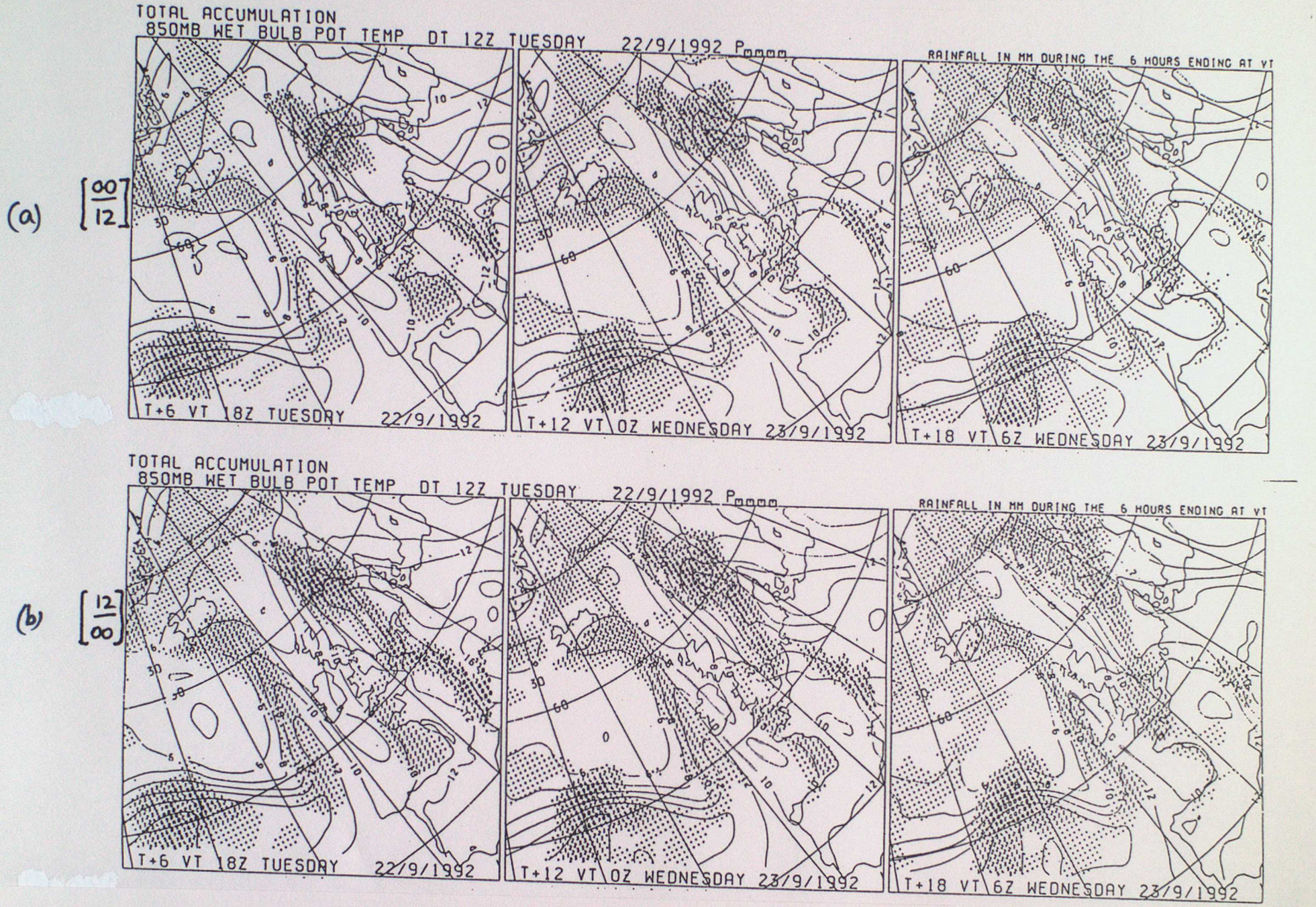

Fig. 20 Forecasts from the LAM of 850 hPa wet-bulb potential temperature (WBPT - isotherms, deg C)) and 6-hourly rainfall accumulations (mm) for the same verifying times as Fig. 8.

(a) Transplant [$\frac{00}{12}$] (b) Transplant [$\frac{12}{00}$].

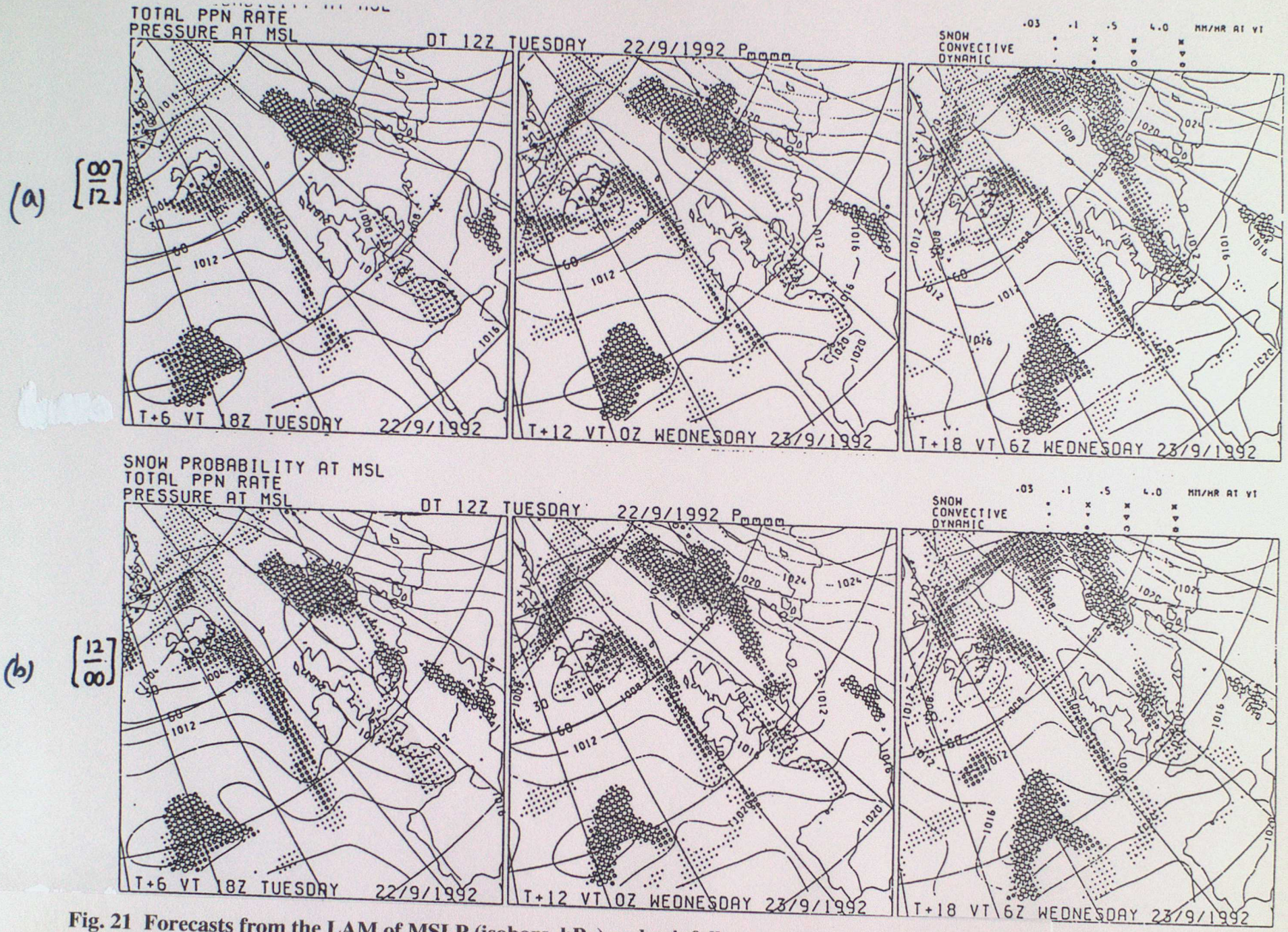

Fig. 21 Forecasts from the LAM of MSLP (isobars, hPa) and rainfall rate (mm per hr) for the same times as Fig. 7.

(a) Transplant [$\frac{00}{12}$] (b) Transplant [$\frac{12}{00}$].

(a)

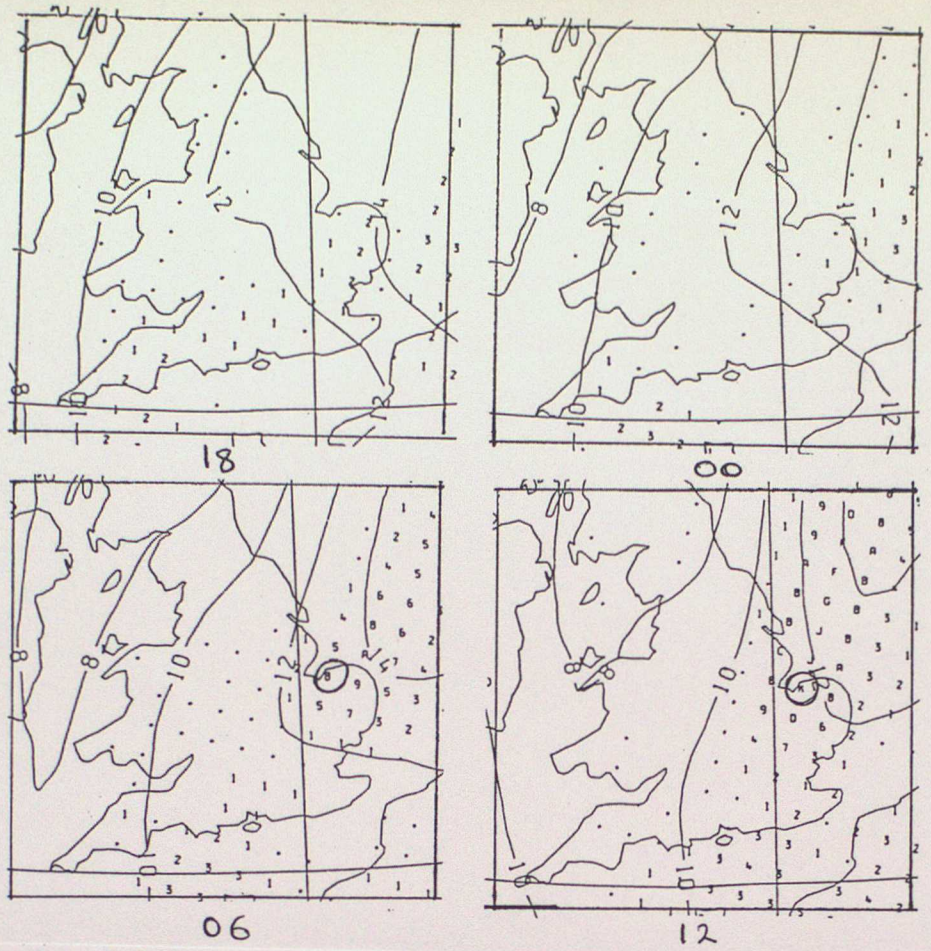

Key to rainfall accumulations for LAM and NMM: in mm to 9; A = 10, B = 11 etc to N = 22, Q = 24, then 5 mm intervals e.g., R = 25-29, X = 55-59, Z = 65 and over.

(b)

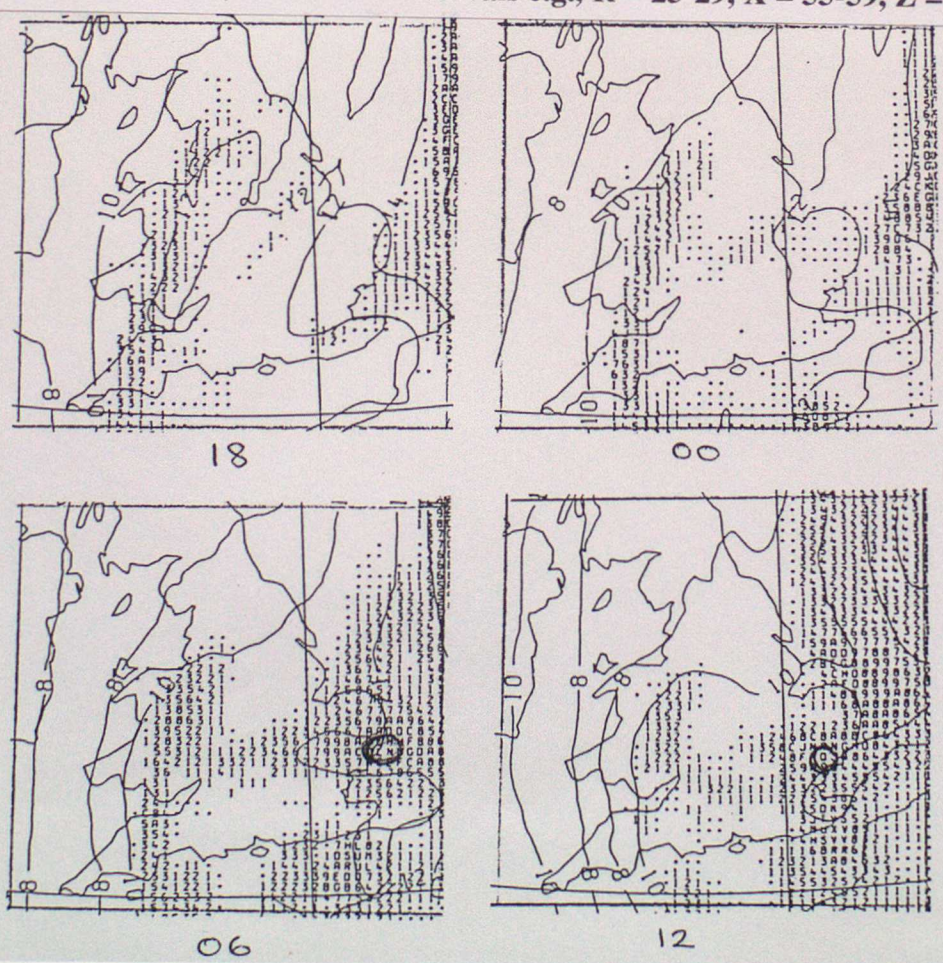

Fig. 22 Forecasts (data time 00 UTC on 22nd September) of WBPT (deg C) at 850 hPa and 6 hour rainfall accumulations (mm) to 18, 00, 06, 12 UTC on 22 - 23 September 1992:

(a) from the the LAM (with new physics),

(b) from the new mesoscale model (NMM).

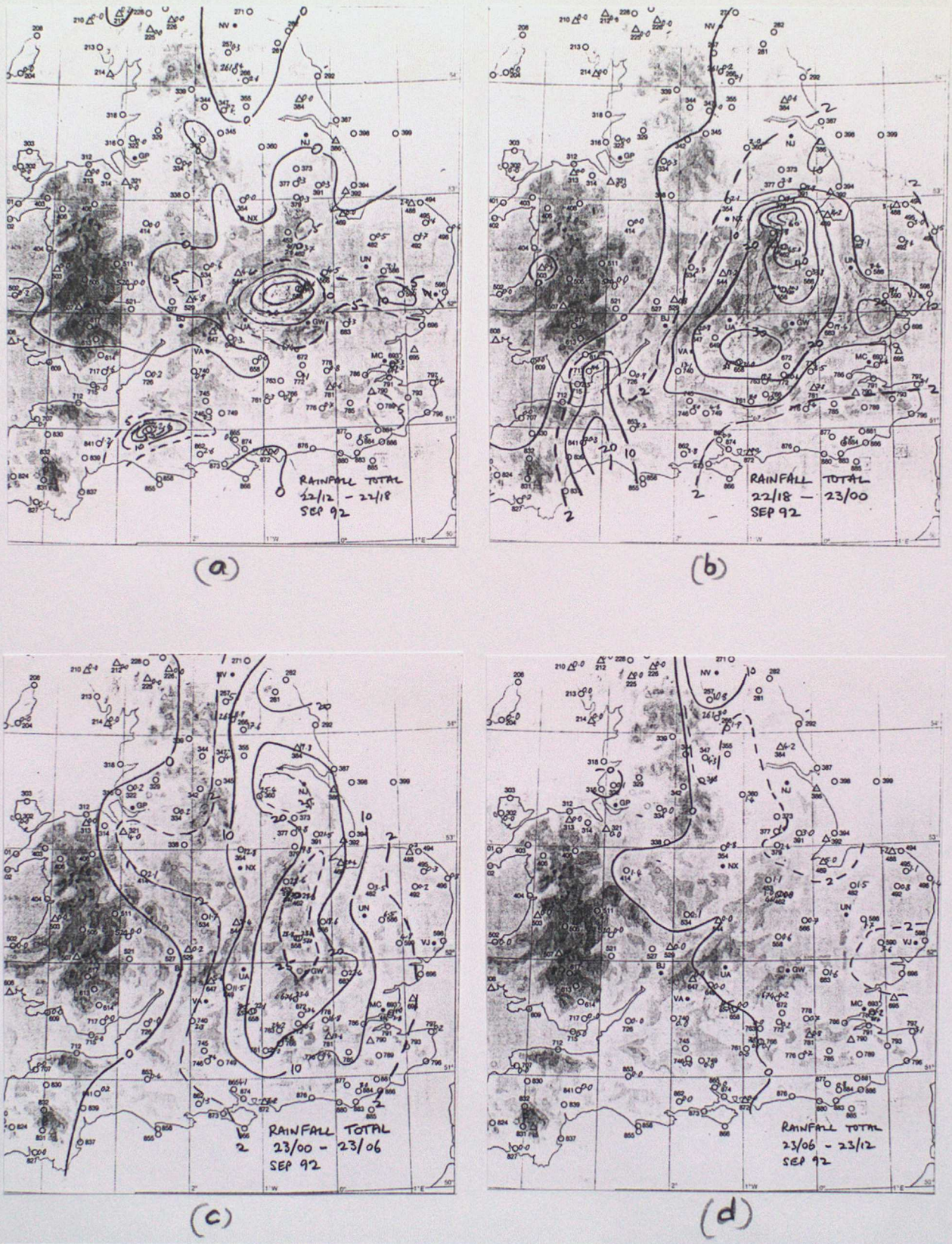

Fig. 23 Observed six-hourly rainfall totals (mm) over the southern part of the UK. Layout as in Fig. 22.
Continuous lines: Totals of 0, 10, 20, 30 and 40 mm
Dashed lines: Totals of 2 mm in (b), (c) and (d), 5 mm in (a).

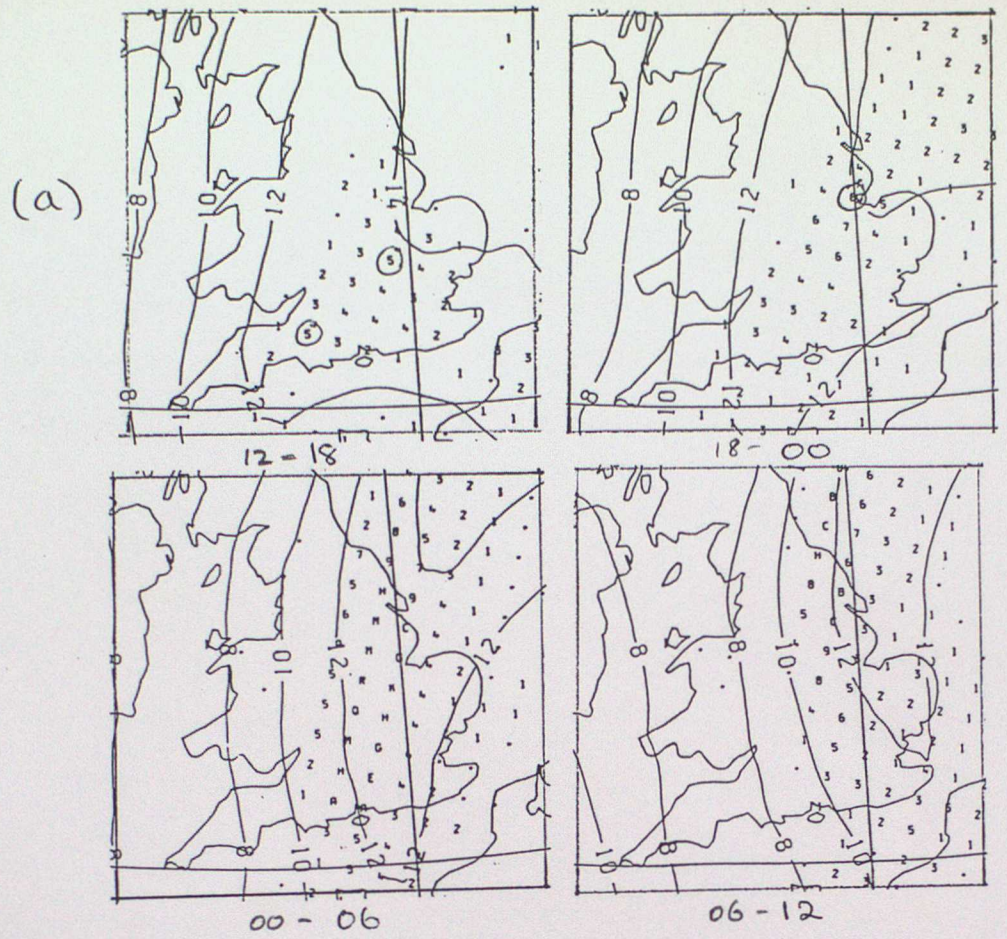

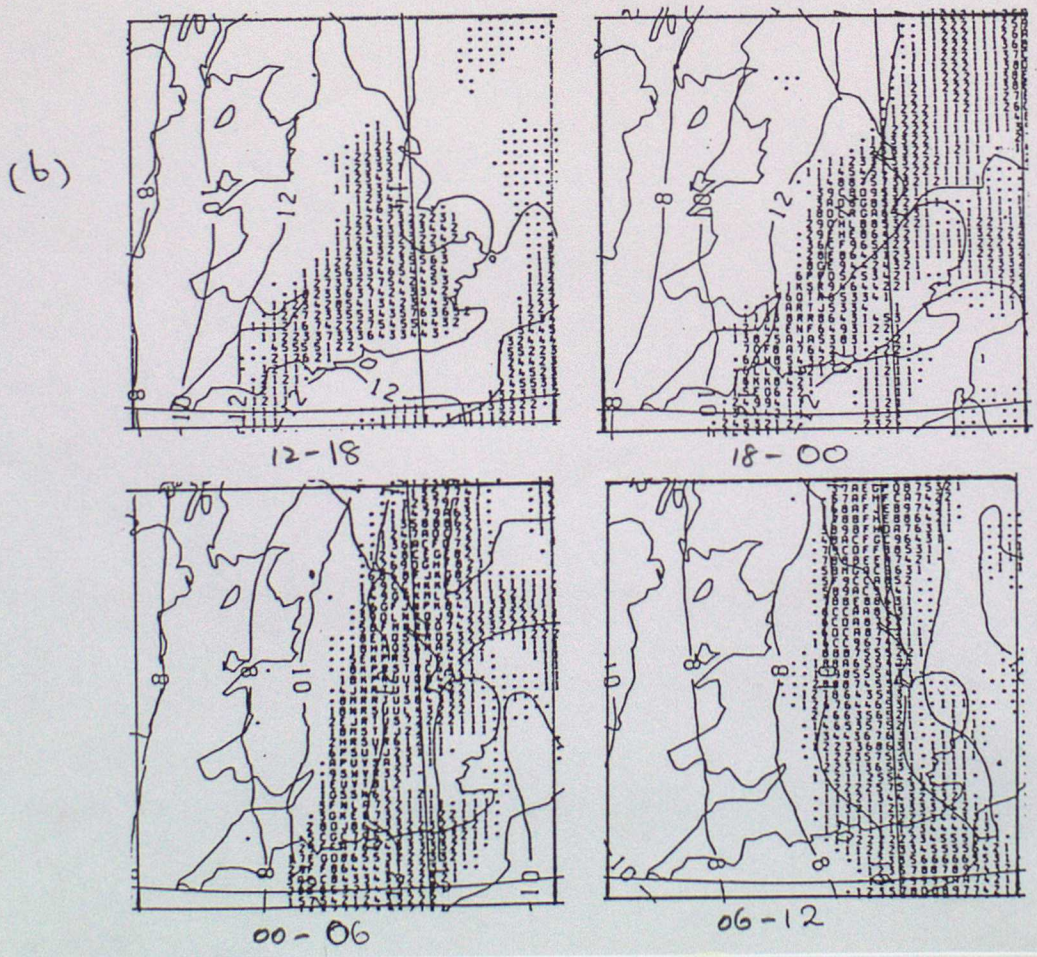

Fig. 24 Forecasts (data time 12 UTC on 22nd September) of rainfall accumulations (mm) and WBPT (deg C) at 850 hPa from (a) the LAM and (b) the new mesoscale model (NMM). Layout as in Fig. 22.

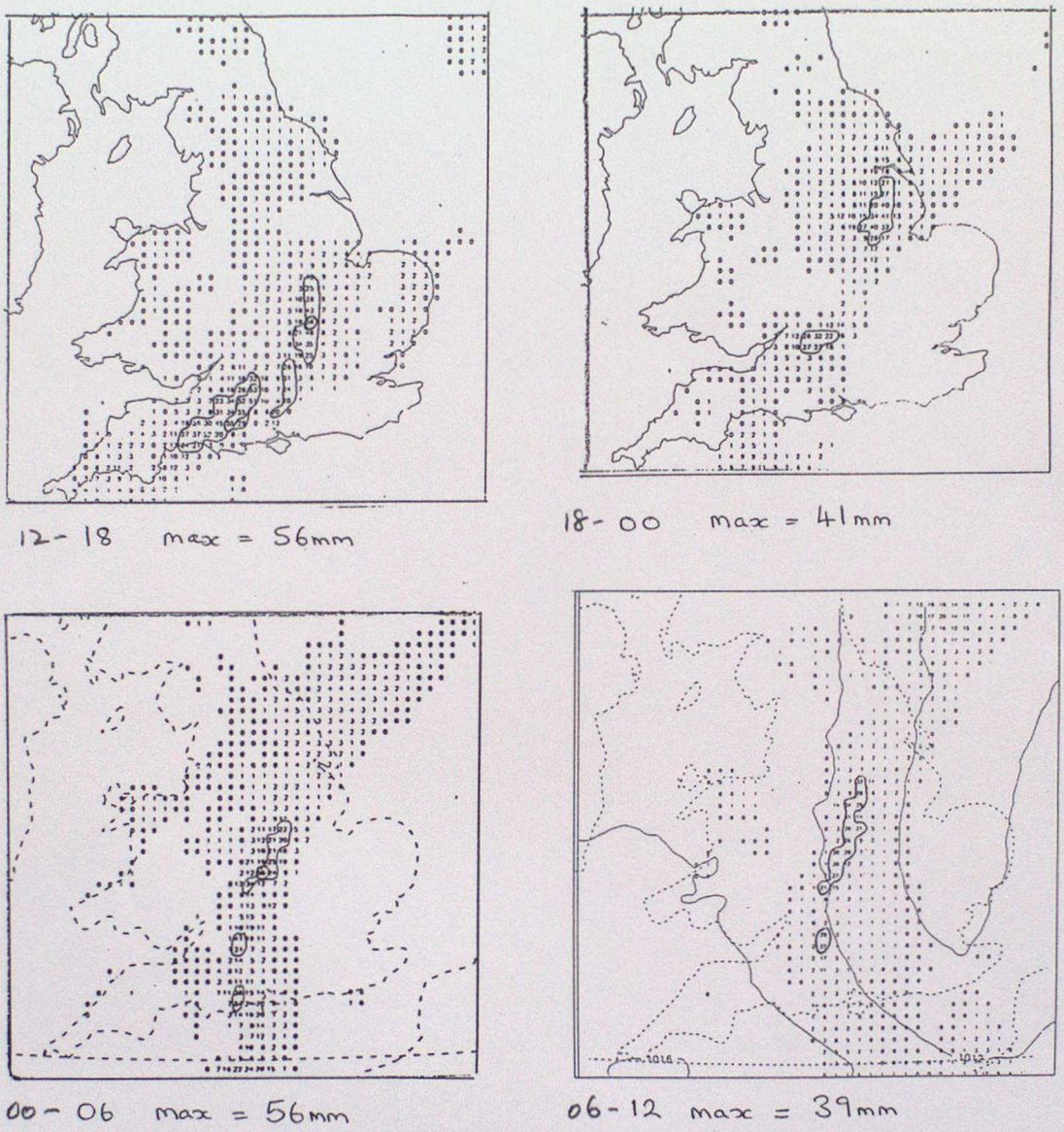

Fig. 25 Forecasts (data time 06 UTC on 22nd September) of rainfall accumulations (mm) from the old mesoscale model (OMM). Layout as in Fig. 22. Isohyets are for totals of 20 and 50 mm. In the bottom right-hand frame, contours are PMSL.

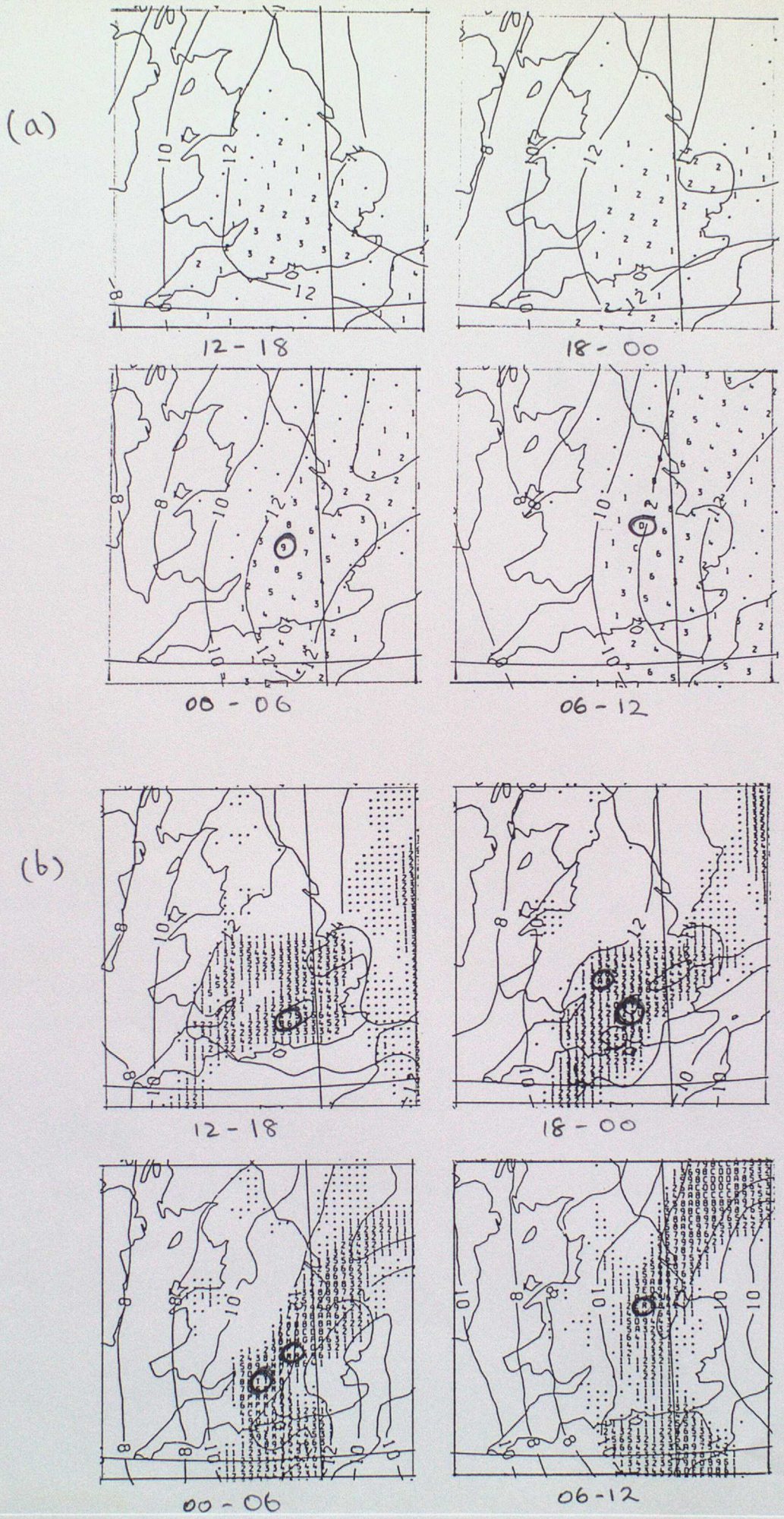

Fig. 26 Forecasts (data time 06 UTC on 22nd September) of rainfall accumulations (mm) and WBPT (deg C) at 850 hPa from (a) the LAM and (b) the new mesoscale model (NMM). Layout as in Fig. 22.

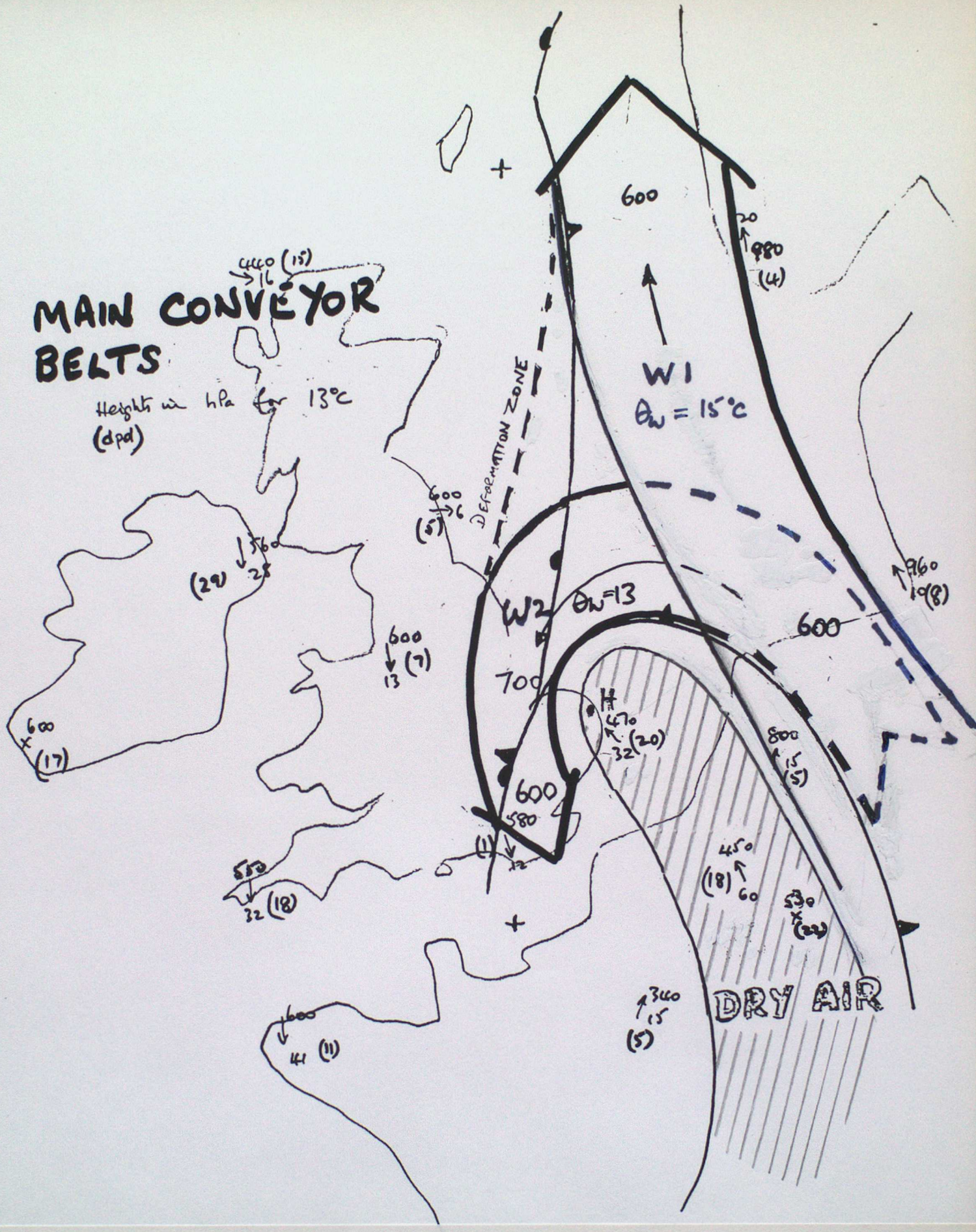

Fig. 27 Conceptual model at 00 UTC on 23rd September 1992 of airflow relative to the surface low (moving at 185 degrees, 12 knots), based on the 13 deg C WBPT surface.

Bold arrows: warm conveyor belts (W1 and W2).

Shading : Dry tongue

Dashed line: deformation zone

Numbers indicate levels (hPa) of the flow.

H indicates Hemsby from where the sounding in Fig. 28 is taken.

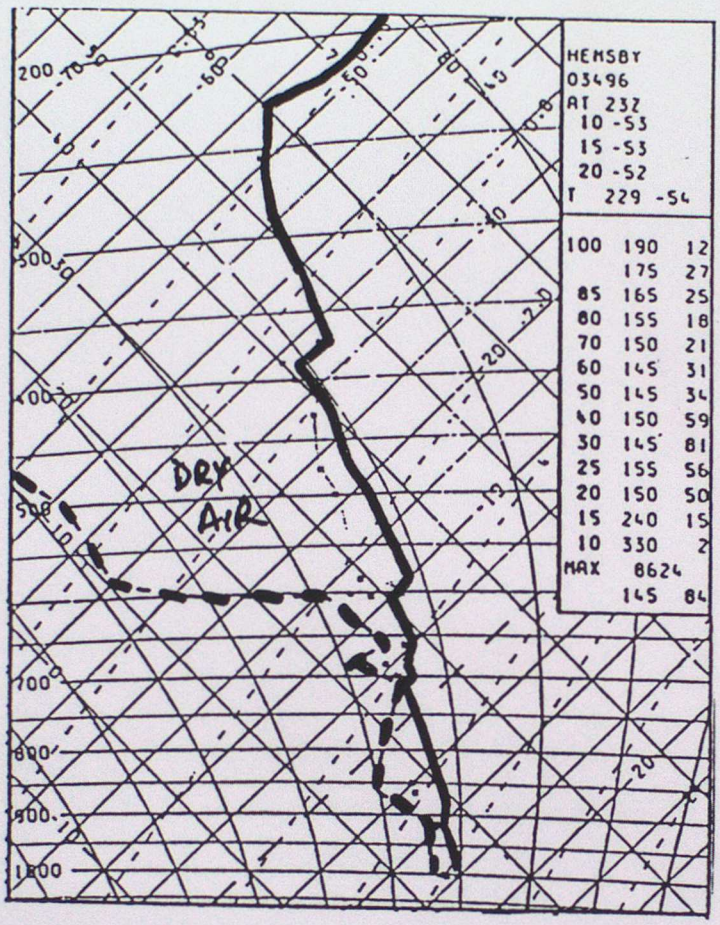

Fig. 28 Radio-sonde ascent for Hemsby at 00 UTC on 23 September 1992 showing dry air above 600 hPa.

APPENDIX
MESOSCALE MODEL FORECASTS: A SENSITIVITY STUDY

A.1 Introduction

A sensitivity study was undertaken with the new mesoscale model and LAM and forecasts were compared with the original non-hydrostatic mesoscale model. The results are reported here and the figures showing forecast 6 hour accumulations should be compared with the observed accumulations shown in figure 23 in the main text. Where forecast accumulations were included as figures in the main text this Appendix will refer back to those figures.

A.2 Original Operational Mesoscale Model Forecasts

The original UK Met Office non-hydrostatic mesoscale model (Golding 1990) was still operational at this time producing two forecasts a day - 18 hours from 00UTC and 30 hours from 06UTC.

The 00UTC 22/9/92 forecast did not produce the observed precipitation to the south east of a line from the Severn Estuary to the Wash in the period 12-18UTC and obviously did not extend to the later periods.

The 06UTC forecast was much better and the model gave good indications of expected high accumulations in the each of the 6 hour periods 12-18UTC 22/9/92, 18-24UTC 22/9/92 and 00-06UTC 23/9/92 , see table A.1 A). The locations of the peak accumulations between 12-18UTC were very good, see figure 25, but the amounts were possibly overdone with a maximum of about 55m compared with peak observed values of 30-40mm. The locations of the peak accumulations were not so good in the following periods being slightly too far to the north and west 18-24UTC, west and south 00-06UTC and south 06-12UTC. Unfortunately the model underdid the precipitation in the South-East and East Anglia. From 03UTC 23/9/92 onwards the forecast did not predict the pivoting of the precipitation band and kept the rain too far west and south than in reality.

A.3 LAM and New Mesoscale Model Forecasts

In July 1991 the Meteorological Office replaced its operational Global and regional (limited area model - LAM) models with versions of a new model, referred to as the Unified Model (Cullen 1991,1993), which is also used as the Climate Model in the Hadley Centre. The Unified Model contains more sophisticated parametrizations of physical processes than the previous larger scale operational models and so is much more similar to the nonhydrostatic mesoscale model and has the additional benefit of a full data assimilation scheme which should remove many of the initialisation problems suffered by the original mesoscale (OMM) forecasting system. Therefore a high resolution version of the Unified Model (NMM) has been developed and this replaced the OMM for the production of operational forecasts for the British Isles area on 8th December 1992 (Ballard et al 1993).

A 6 hour assimilation and 30 hour forecast for data time 06UTC 22/9/92 was run to check that the new model can predict high rainfall accumulations and provide the same benefit as the OMM compared with the LAM. The 06UTC LAM assimilation and forecast was rerun (LAMNP) using the physics operational after 27/4/93 to provide boundary conditions for the NMM assimilation and forecast. The NMM was run using the same physics as the LAMNP, 4th order horizontal diffusion and the mesoscale roughness length scheme. Initially MOPS data (Wright 1993, Macpherson et al 1993) was not included.

The LAMNP forecast, see figure 26a), was very similar to the operational LAM forecast but accumulations were decreased slightly in the 12-18UTC period and increased slightly in the later periods, see table A.1 C) compared with B).

The NMM , see figure 26b) and table A.1 D), gave a good indication of expected high rainfall accumulations and the location of some of the peak values in the later stages of the forecast and in all periods accumulations were significantly higher than the LAMNP. However in the period 12-18UTC the accumulations were significantly lower than the OMM and observations possibly indicating increased problems with spin-up in the precipitation forecasts from the NMM compared with the OMM. The location of the rainfall was slightly better in the NMM than the OMM as it spread the rain slightly further east, see figure 26b), however neither model spread the area of significant accumulations far enough into East Anglia.

The LAM with new physics and NMM were also rerun from 00UTC and 12UTC LAM analyses to investigate the impact of higher resolution on those forecasts. The 00UTC forecasts were similar to the operational LAM and had the same deficiencies although accumulations were higher in the NMM, see figure 22 and table A.1 F),G) and H). Again for the 12UTC runs the forecasts were similar to the operational LAM and the accumulations were higher in the NMM, see figure 24 and table A.1 I),J) and K).

A.4 Impact of data and data assimilation

A few extra sensitivity studies were run for the 06UTC 22/9/92 forecasts which tested the impact of the 06UTC data on the improvement of the 06UTC forecasts over the 00UTC forecasts. The NMM forecast was rerun without assimilating data, NMMNA, and, as can be seen from figure A.1a) and table A.1 N), the high accumulations in the period 12UTC to 24UTC are far better forecast than from the 00UTC forecast. The peak accumulations also occur further east, and are possibly better placed, than in the forecast with data assimilation. Therefore there is an improvement in the 06UTC forecasts over the 00UTC forecasts other than just from the inclusion of the 06UTC data (which may in fact have shifted the precipitation too far west).

The 06UTC NMM and LAM assimilation and forecasts involve interpolating the 00UTC global analysis onto the respective model grids and running forward with assimilation of data for the first 8 and 9 hours respectively, the LAM taking its boundary conditions from the 00UTC global forecast and the NMM from the 06UTC LAM assimilation and forecast. Therefore as well as including later data from the period 00UTC to 06UTC

the 06UTC forecasts are also based on the 00UTC global analysis and boundary conditions rather than the 00UTC LAM. For completeness the 06UTC LAM was also run without data assimilation, ie from the 00UTC global analysis and boundary conditions (LAMGA, table A.1 L) as opposed to the operational 00UTC LAM forecast, and LAMNP, which were run from the 00UTC LAM analysis with boundary conditions from the 12UTC 21/9/92 global forecast. By comparing figures A.2a) and 22a) it can be seen that there is a great improvement in the timing and location of the precipitation in the forecast from the 00UTC global analysis and boundary conditions.

The NMM without data assimilation was also run using boundary conditions from the LAMGA, there were differences from NMMNA showing some impact from the boundary conditions but the forecasts were closer than between NMMNA and the NMM from 00UTC LAM analysis, see figure A.2b) and table A.1 M).

Operationally MOPS data is included in the mesoscale forecasts so the 06UTC forecast was rerun including this data to see if it could increase the accumulations in the period 12-18UTC. As can be seen from table A.1 Q) there was a slight but insignificant increase. The general distribution of the precipitation was similar to D) but the peak intensities and locations were slightly different as can be seen by comparing figures 26b) and A.4a).

A.5 Sensitivity to convection scheme

It was found that the timing of the peak accumulations in NMMNA and distribution of the precipitation was sensitive to details of the convection scheme. Initially the operational NMM was run with higher values of some parameters in the scheme than the LAM and climate models (On 14th September 1993 the NMM was changed to use the same values as the LAM and as were used in the NMM runs described above). Increases in these parameters increase the initial parcel mass flux and its bouyancy excess over environmental values ie make the convection more likely to trigger, possibly make it more vigorous, and result in differences in vertical mixing. The 06UTC NMMNA was rerun using the original operational values and it was found that the time of peak accumulations shifted from before midnight to after midnight, see figure A.3 and table A.1 P). Intermediate values of the parameters resulted in intermediate impact on the timing of the precipitation as can be seen from figure A.1b) and table A.1 O). The impact of changes in these parameters was less marked when data assimilation was included.

A.6 Sensitivity to horizontal diffusion

It was noticed that in all the mesoscale forecasts the very high accumulations were associated with isolated regions of high upward vertical velocities at 700 and 850 hPa, compare figures A.4a) and A.5a) . These appeared somewhat unrealistic and distorted the precipitation fields and 850 hPa wet bulb potential temperature fields compared with the LAM forecasts. Q) was rerun but using the second order horizontal diffusion as initially used operationally in the NMM rather than the 4th order diffusion as used in the LAM (and in the NMM operationally after 14th September 1993). As can be

seen from table A.1 R) this reduced the peak accumulations slightly and reduced the vertical velocities so that the fields were smoother, see figure A.5b), but the general distribution of precipitation was the same, see figure A.4b). This is what would be expected as the 4th order diffusion was introduced operationally because it produces sharper gradients and less smoothing. It is possible that a slightly higher diffusion coefficient is needed with the 4th order diffusion to dampen some of these regions of vigorous ascent. Currently the effect of mass loading of cloud water and precipitation is excluded from the unified model dynamics , if this was included it may also reduce the vertical velocity. However from figure 23 it can be seen that the observed peak accumulations do appear to have occured in isolated regions and it could be argued that the forecasts with 4th order diffusion are more realistic.

A.7 Initial operational version of new mesoscale model

Finally some of the mesoscale forecasts were repeated using the initial operational formulation, ie 2nd order diffusion and increased convection parameters. The peak accumulations from these forecasts are shown in table A.2. It can be seen in many of the forecasts that the peak values have decreased as a result of the 2nd order diffusion producing smoother fields but the general conclusions are the same. Forecasts N2,O2,P2 produced less precipitation in the west, particularly over Wales, and in the NW-SE band at 06-12UTC than N,O and P.

A.8 Comparison of instantaneous surface precipitation rates

Figures A.6 to A.10 compare the distribution of the FRONTIERS composite radar derived precipitation rates with the forecast surface precipitation rates from the 06UTC OMM and Q2 (original operational configuration of NMM), Q (configuration of NMM after 14/9/93) and R (as Q but 2nd order diffusion).

The change from the morning and afternoon convective precipitation to more organised band of precipitation overnight can be seen to some extent in all the forecasts. All the NMM forecasts have a greater eastward extent of precipitaion, mainly convective than the OMM. Q improves the distribution of convection in the morning and afternoon compared with Q2 but suffers overnight due to the production of regions of intense vertical velocity and precipitation. As expected R is smoother than Q, the convection is probably too widespread during the afternoon but does not suffer from the isolated regions of intense precipitaion overnight.

In figure A.11 the evolution of the precipitation rates in forecast O) are shown to illustrate the more eastern location of the precipitation in the 06UTC runs without data assimilation, ie from the 00UTC global analysis.

A.9 Conclusions

Possibly the best forecast was the 06UTC forecast from the old mesoscale model which gave a good indication of expected high accumulations of precipitation in all 4 6-hour periods from 12UTC 22/9/92 to 12UTC 23/9/92. This was the only forecast to indicate high accumulations in the period 12-18UTC. The locations of the peak

accumulations were reasonable but suffered from too little precipitation in the east and a slight westward displacement. As with all forecasts there was too little rotation of the precipitation band in the later stages of the forecast.

The new mesoscale model forecasts followed the general evolution of the LAM but provided added detail and higher accumulations. None of the unified model forecasts predicted the high accumulations in the afternoon of the 22/9/92 and were poorer than the OMM in this respect. However they did correctly extend the precipitation further eastwards.

There was sensitivity in the unified model forecasts to the data assimilation (ie analyses), physical parametrisations and horizontal diffusion.

The location of the precipitation band seemed to move progressively westward in forecasts run from the 00UTC LAM, 00UTC global, 06UTC LAM/mesoscale analyses. The reason for the improvement between the 00UTC LAM and 00UTC global analyses should be investigated.

The timing of peak accumulations of precipitation was seen to depend on the formulation of the convection scheme and the intensities on the amount of smoothing produced by horizontal diffusion. Reduced diffusion and convection parameters produced possibly more realistic distributions of convection but the reduced diffusion possibly produced excessive precipitation accumulations and hence evaporative cooling.

REFERENCES

Ballard, S.P., Robinson, R., Barnes, R.T.H., Jackson, S. and Woltering S. 1993 'Development and performance of the new mesoscale model' , Forecasting Research Technical Report No 40.

Cullen, M.J.P. 1991, 'The Unified Forecast/Climate Model', Short Range Forecasting Research Scientific Paper No 1.

Cullen, M.J.P. 1993, 'The Unified Forecast/Climate Model', Meteorological Mag., 122, 81-94.

Golding, B. 1990, 'The Meteorological Office mesoscale model.', Meteorological Mag. 119 81-96.

Lorenc, A.C., Bell, R.S. and Macpherson, B. 1991, 'The Meteorological Office analysis correction data assimilation scheme.' Q.J.R. Meteorol. Soc., 177, 59-89.

Macpherson, B., Wright, B.J. and Maycock A.J. 1993, ' Performance of the data assimilation scheme in the operational trial of the new mesoscale model.', Forecasting Research Div. Technical Report No 39.

Wright, B.J. 1993, 'The Moisture Observation Pre-processing System.' Forecasting Research Technical Report No 38.

Table A.1: Comparison of peak 6-hour accumulations of precipitation in mm between old mesoscale model, operational LAM, LAM with new physics introduced on 27/4/93 and new mesoscale model forecasts (using LAM convection parameters and 4th order horizontal diffusion).

	PEAK 6-HOUR ACCUMULATIONS OF PRECIPITATION IN mm			
	22/9/92		23/9/92	
	12-18UTC	18-24UTC	00-06UTC	06-12UTC
OBSERVED	42.4	45.0	28.5	15.0
FORECAST				
A) 06UTC OP MES	56	41	56	39
B) 06UTC OP LAM	3	1	7	9
C) 06UTC LAM new physics	3	2	9	13
D) 06UTC new Mesoscale #	8	>65	35-59	25-29
E) 00UTC OP MES	27(Wales)	-	-	-
F) 00UTC OP LAM	1	1	11	19 or 22
G) 00UTC LAM new physics *	2	1	11	19
H) 00UTC new Mesoscale # *	2/10(SW)	1/8(SW)	14	25-29
I) 12UTC OP LAM	4	8	23	13
J) 12UTC LAM new physics *	5	7	25-29	17
K) 12UTC new mesoscale # *	8	35-39	50-54	17
L) 06UTC LAM new physics, no assim ie 00UTC global analysis	4(SW)	3	7	13
M) 06UTC new mesoscale # no assim,00UTC global anal and L) b.c	7	40-44	9	9
N) as M) but C) b.c.	6	50-54	12	16
O) as N) but intermediate conv params	7	60-64	20	13
P) as N) but original op conv params	10	25-29	50-54	15
Q) as D) but MOPS included	9	17	50-54	20
R) as Q) but 2nd order diffusion	9	7	30-34	16

* forecast only rerun from operational LAM analysis
# using mesoscale surface roughness scheme, LAM new physics (ie climate/LAM convection params) and 4th order horizontal diffusion but no MOPS data

Table A.2: Comparison of peak 6-hour accumulations of precipitation in mm between old mesoscale model, operational LAM, LAM with new physics introduced on 27/4/93 and new mesoscale model forecasts (using 2nd order horizontal diffusion and mesoscale convection parameters)

	PEAK 6-HOUR ACCUMULATIONS OF PRECIPITATION IN mm			
	22/9/92		23/9/92	
	12-18UTC	18-24UTC	00-06UTC	06-12UTC
OBSERVED	42.4	45.0	28.5	15.0
FORECAST				
A) 06UTC OP MES	56	41	56	39
B) 06UTC OP LAM	3	1	7	9
C2) 06UTC LAM mes physics "	6	5	10	8
D2) 06UTC new Mesoscale #	5	6	25-29	10
E) 00UTC OP MES	27(Wales)	-	-	-
F) 00UTC OP LAM	1	1	11	19 or 22
G) 00UTC LAM new physics *	2	1	11	19
H2) 00UTC new Mesoscale # *	4	3	17	10
I) 12UTC OP LAM	4	8	23	13
J) 12UTC LAM new physics *	5	7	25-29	17
K2) 12UTC new mesoscale # *	7	17	30-34	13
L) 06UTC LAM new physics, no assim ie 00UTC global analysis	4(SW)	3	7	13
N2) 06UTC new mesoscale no assim,00UTC global anal C2) as bc, climate/LAM convection parameters	6	>65	19	16
O2) as N2) but intermediate conv params	6	55-59	25-29	12
P2) as N2) but original op conv params	7	7	60-64	14
Q2) as D2) but mops included	6	7	30-34	7

* forecast only rerun from operational LAM analysis
# using mesoscale surface roughness scheme, new physics with original operational convection params and 2nd order horizontal diffusion but no MOPS data
" run using LAM new physics but original mesoscale convection parameters

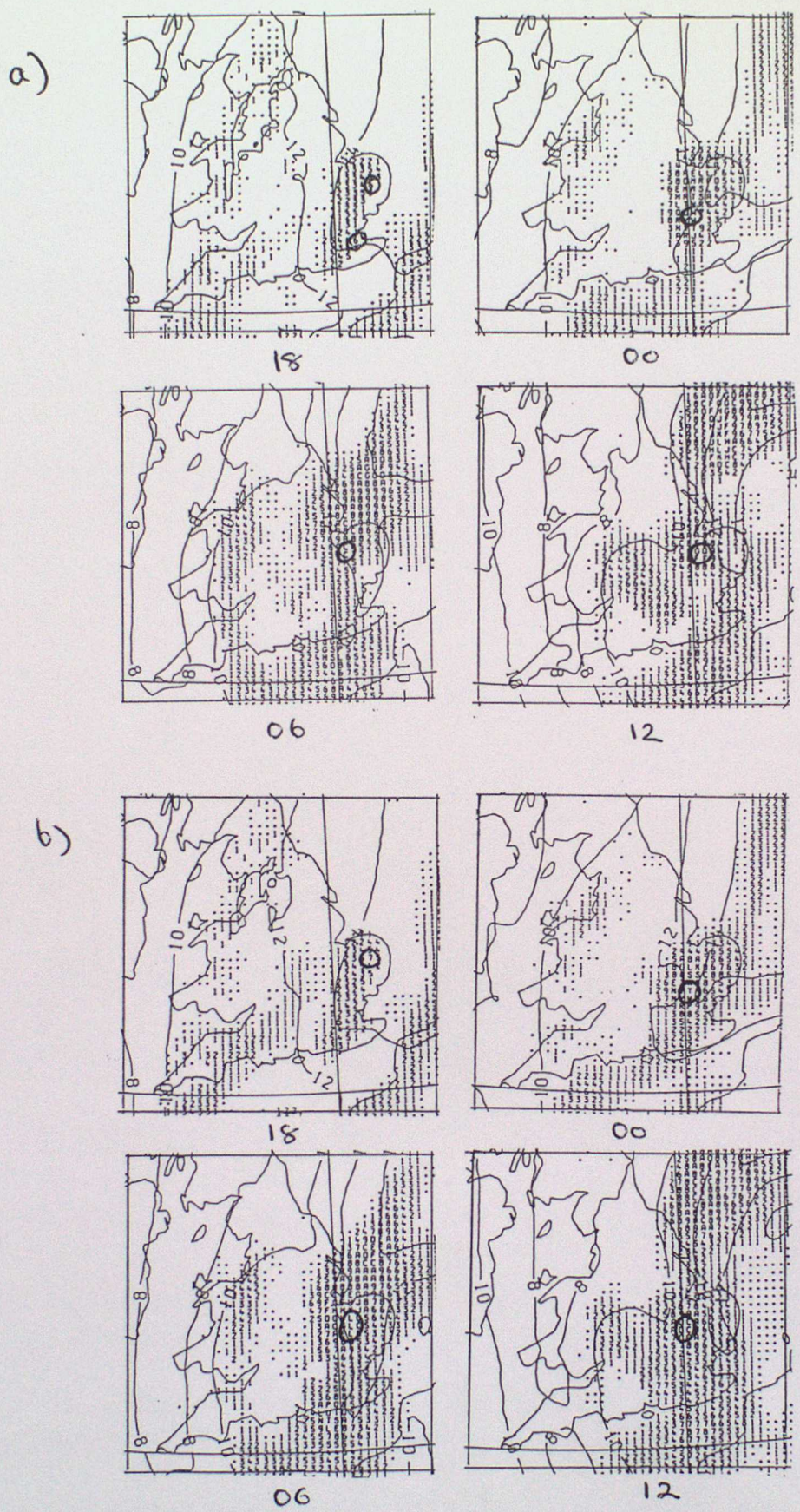

FIGURE A.1 Forecasts of WBPT (deg C) at 850 hPa and 6 hour rainfall accumulations (mm) to 18, 00, 06, 12 UTC on 22-23 September 1992. Locations of peak accumulations are ringed: a) New mesoscale model with no assimilation and climate/LAM convection parameters (NMMNA). Forecast N) in table A.1 run from 00UTC global analysis with boundary conditions from 06UTC LAM (C) assimilation and forecast. b) As a) but with intermediate convection parameters. Forecast O) in table A.1

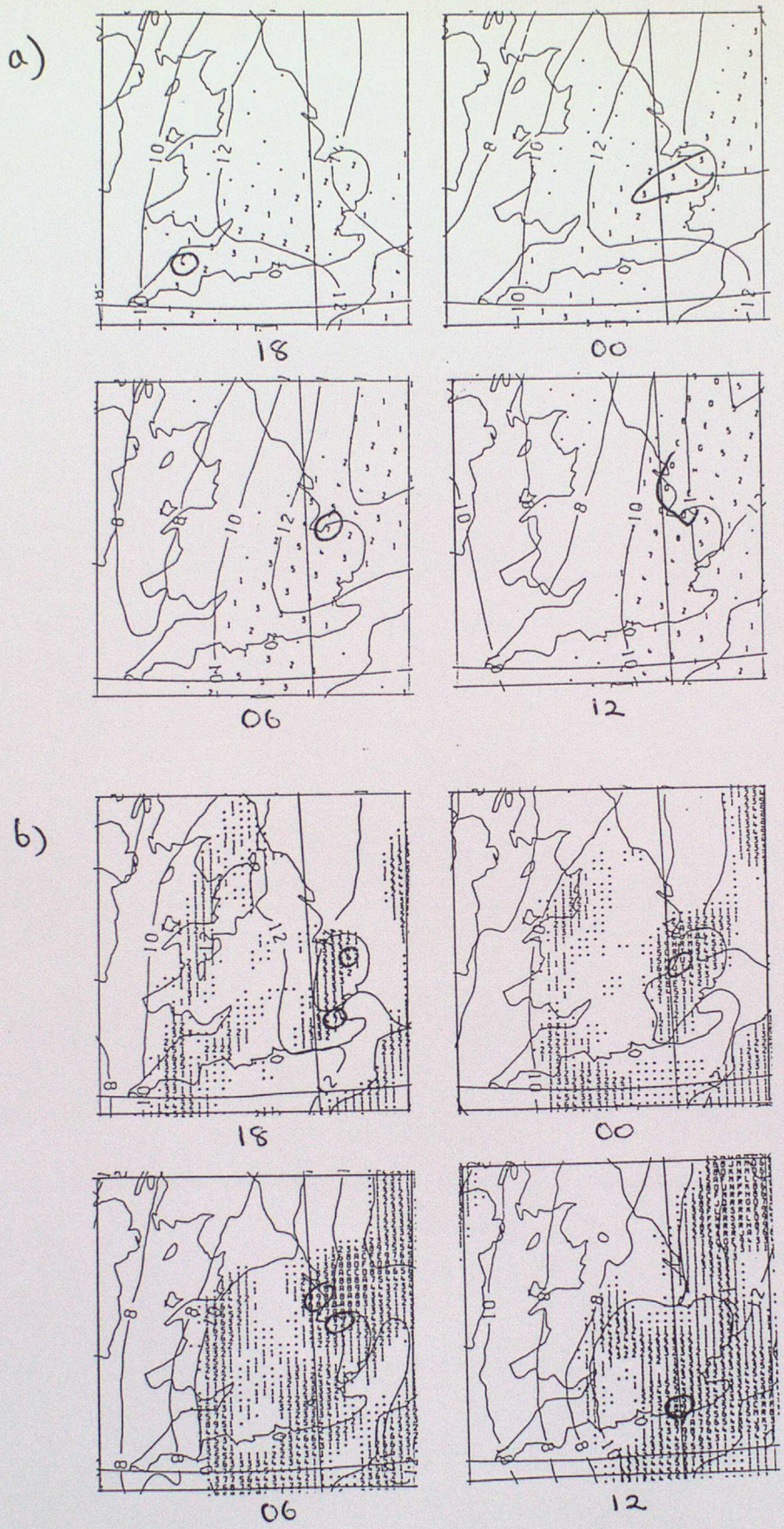

FIGURE A.2 Forecasts of WBPT at 850 hPa and 6 hour rainfall accumulations. Layout as figure A.1. a) LAM with no assimilation (LAMGA). Forecast L) in table A.1 run from 00UTC global analysis and boundary conditions
b) NMM with no assimilation. Forecast M) in table A.1 run from 00UTC global analysis and boundary conditions from a).

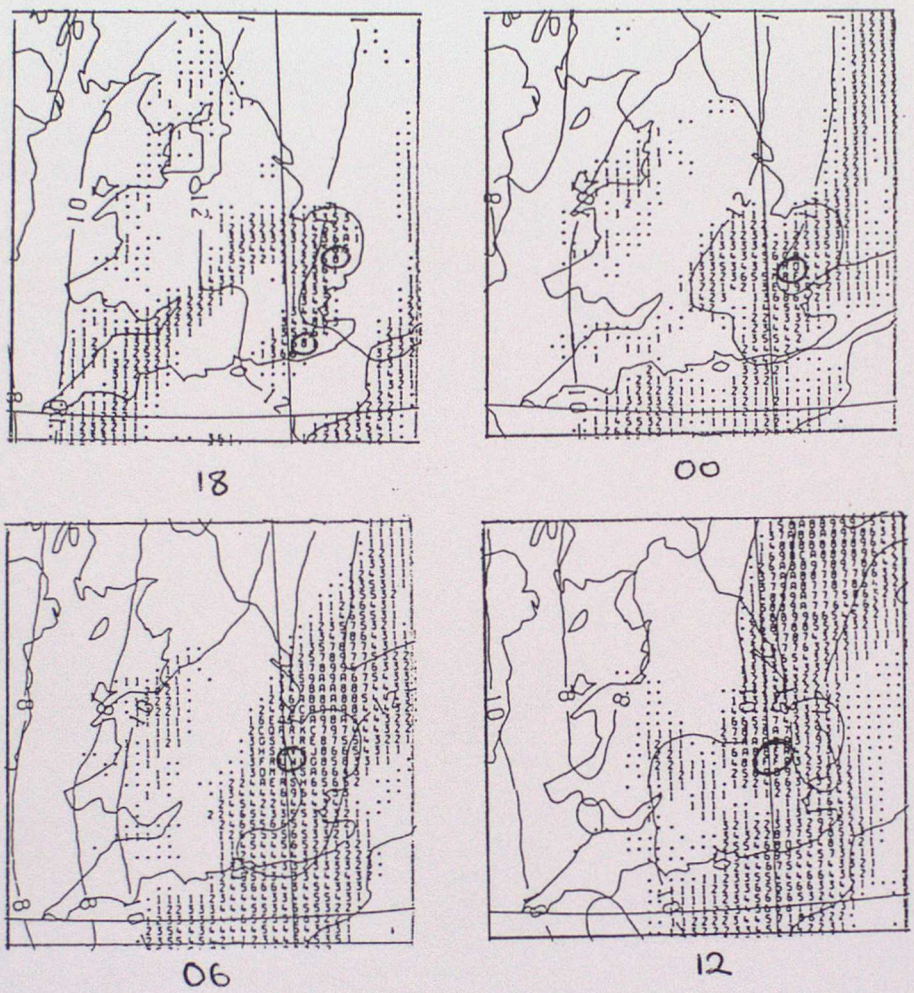

FIGURE A.3 Forecasts of WBPT at 850 hPa and 6 hour rainfall accumulations. Layout as figure A.1. NMM As figure A.1a) but with original operational convection parameters. Forecast P) in table A.1

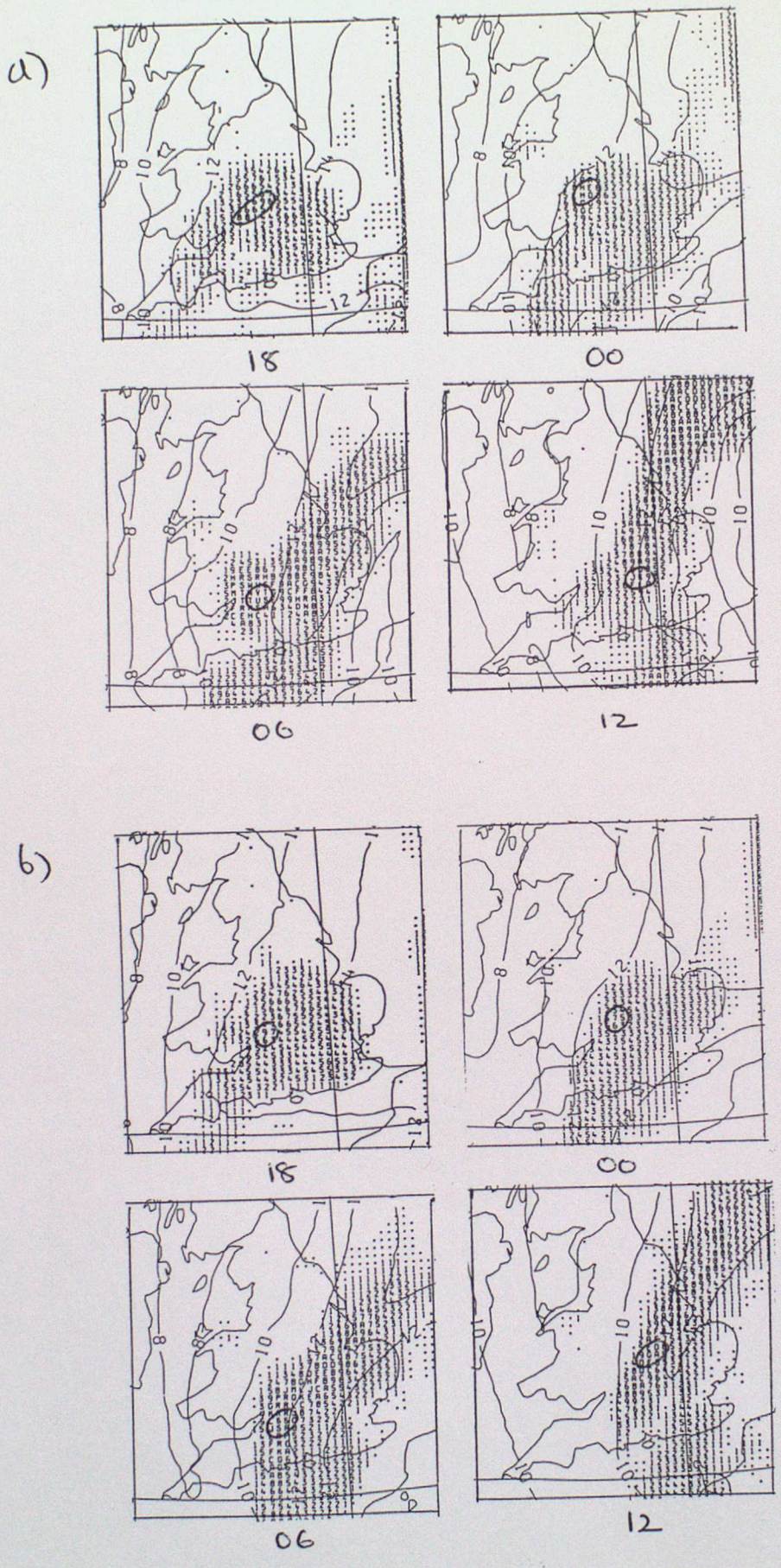

FIGURE A.4 Forecasts of WBPT at 850 hPa and 6 hour rainfall accumulations. Layout as figure A.1. a) 06UTC NMM with assimilation including MOPS data and 4th order horizontal diffusion. Forecast Q) in table A.1.
b) As a) but with 2nd order horizontal diffusion. Forecast R) in table A.1

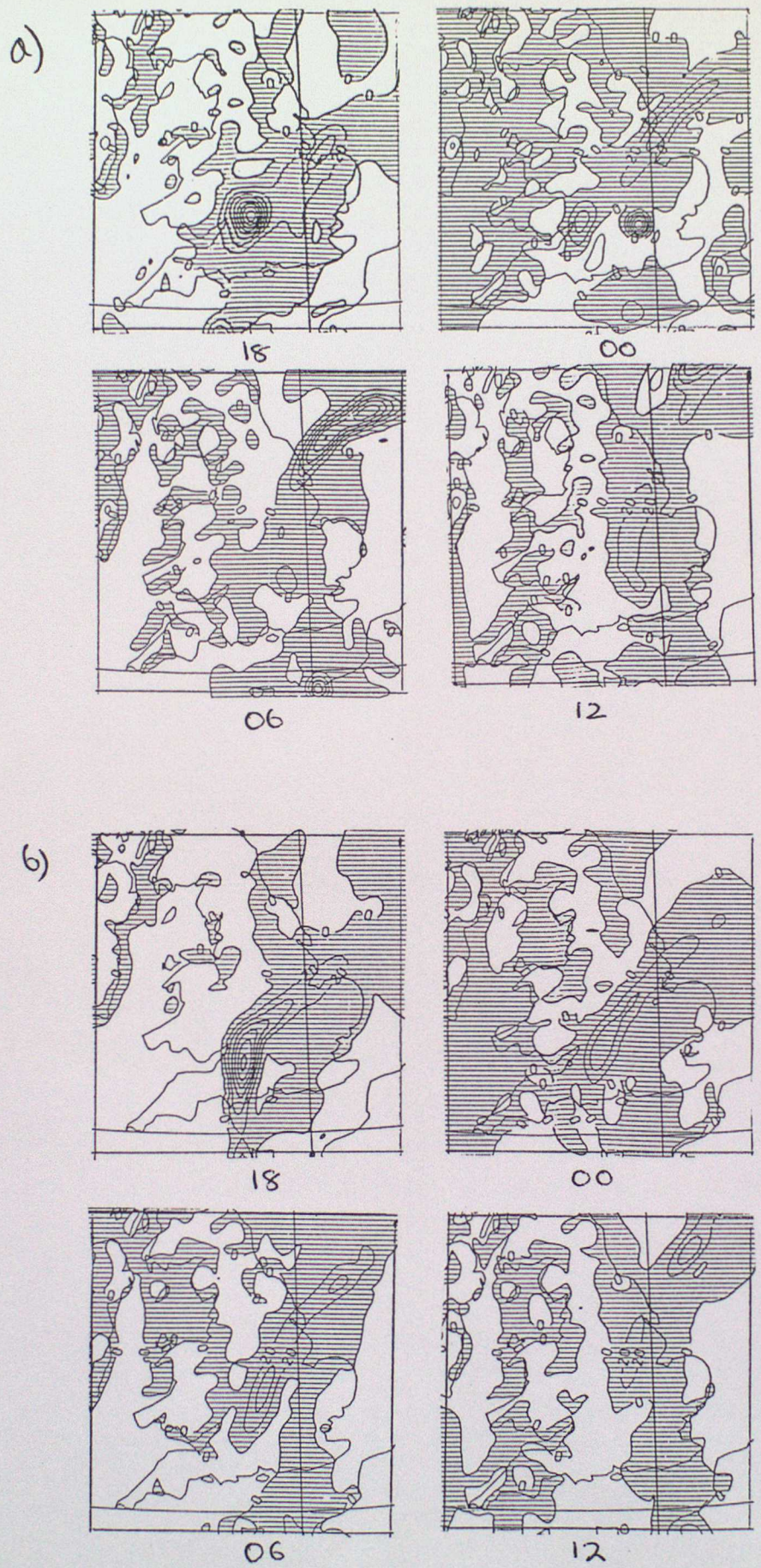

FIGURE A.5 Forecasts of 700 hPa vertical velocity for 03UTC, 06UTC, 09UTC and 12UTC 23 September 1992. a) 06UTC NMM with assimilation including MOPS data and 4th order horizontal diffusion. Forecast Q) in table A.1.
b) As a) but with 2nd order horizontal diffusion. Forecast R) in table A.1

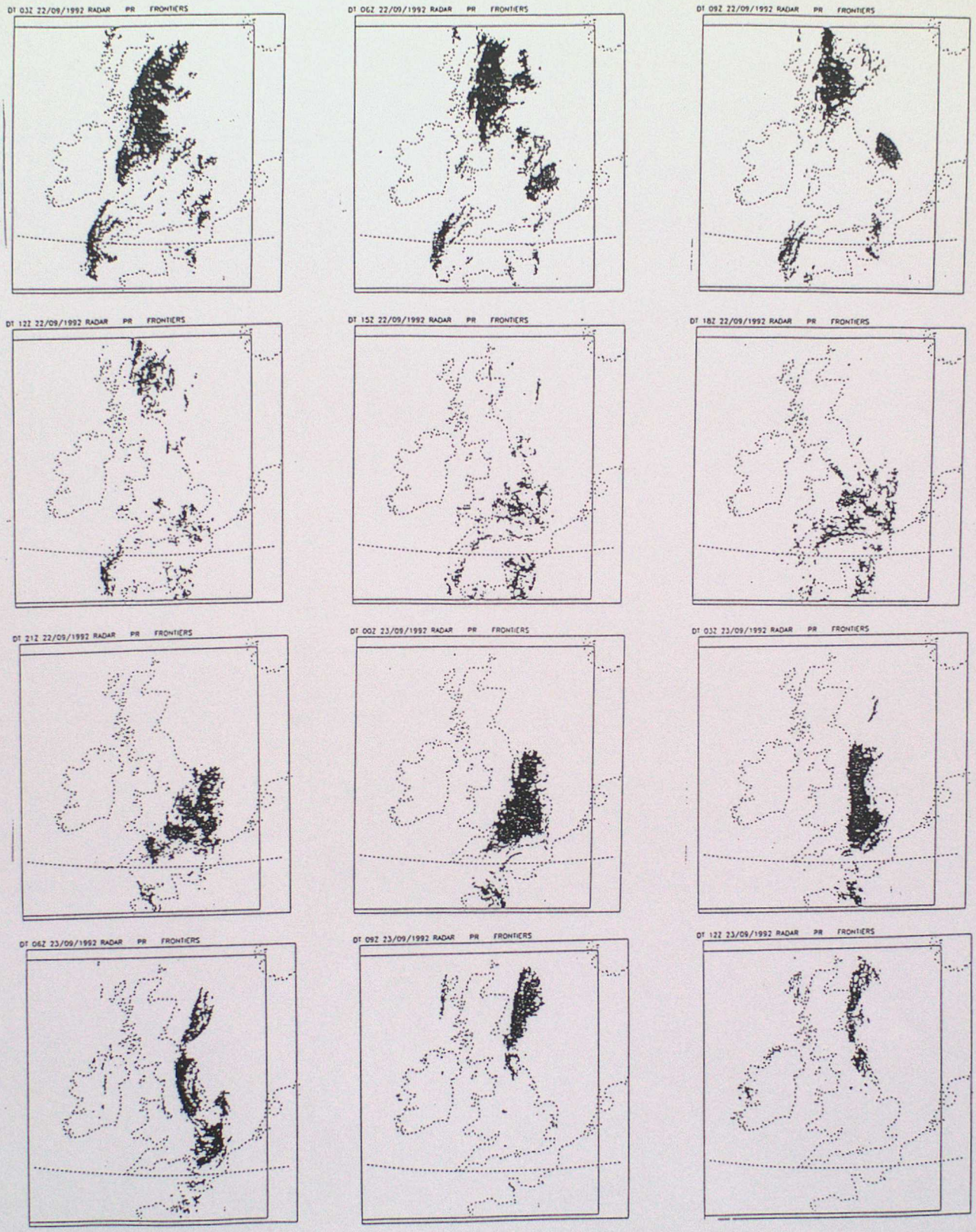

FIGURE A.6 Location of surface precipitation as observed by FRONTIERS radar 03UTC 22 September 1992 to 12UTC 23 September 1992 at 3 hourly intervals.

FIGURE A.7 Forecast precipitation from OMM data time 06UTC 22 September 1992 at 3 hourly intervals from 06UTC 22 September 1992 to 12UTC 23 September 1992. Forecast A) in table A.1

FIGURE A.8 Forecast precipitation and mean sea level pressure from NMM data time 06UTC 22 September 1992 at 3 hourly intervals from 03UTC 22 September 1992 to 12UTC 23 September 1992. Forecast Q2) in table A.2

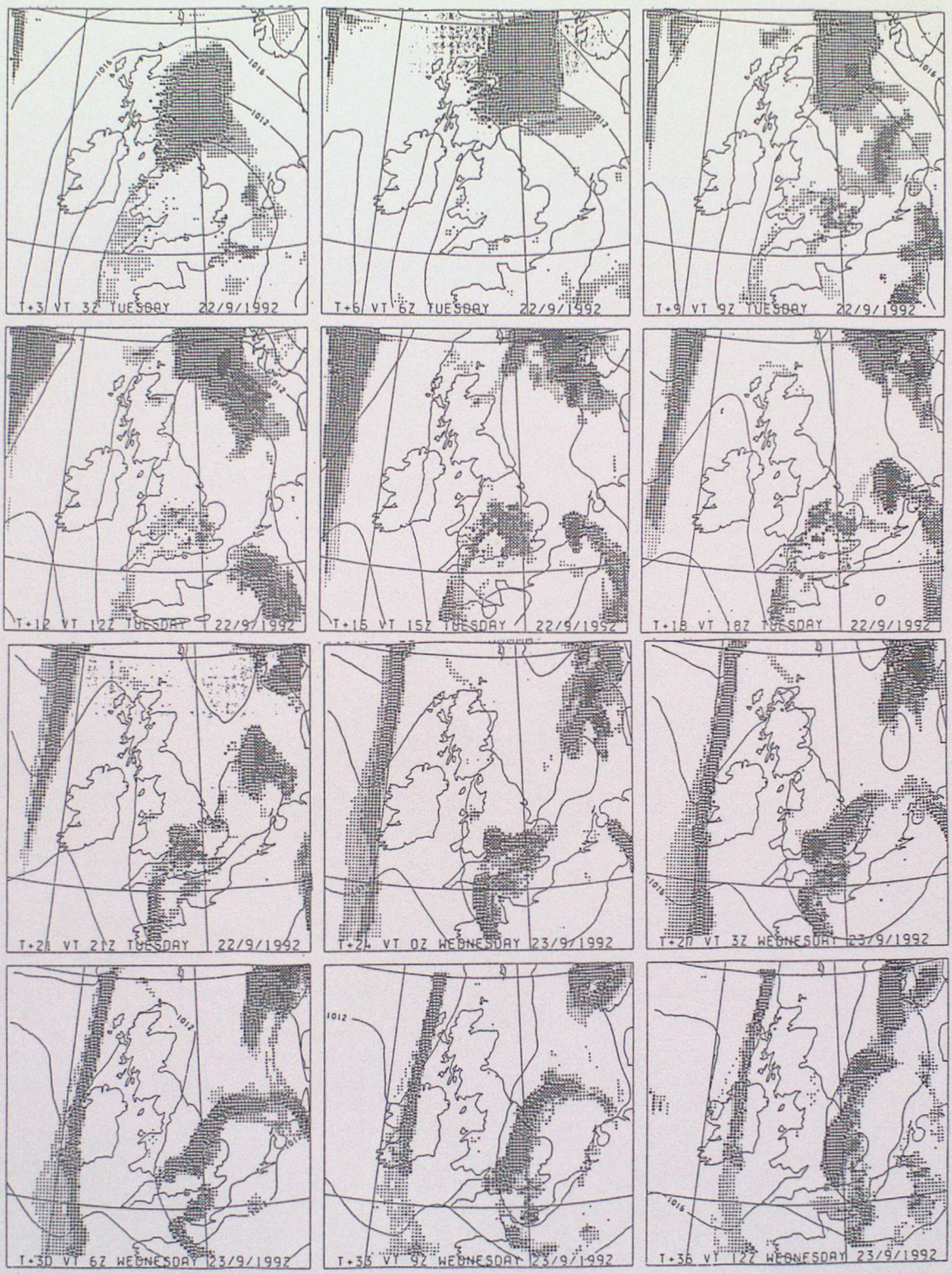

FIGURE A.9 Forecast precipitation and mean sea level pressure from NMM data time 06UTC 22 September 1992 at 3 hourly intervals from 03UTC 22 September 1992 to 12UTC 23 September 1992. Forecast Q) in table A.1

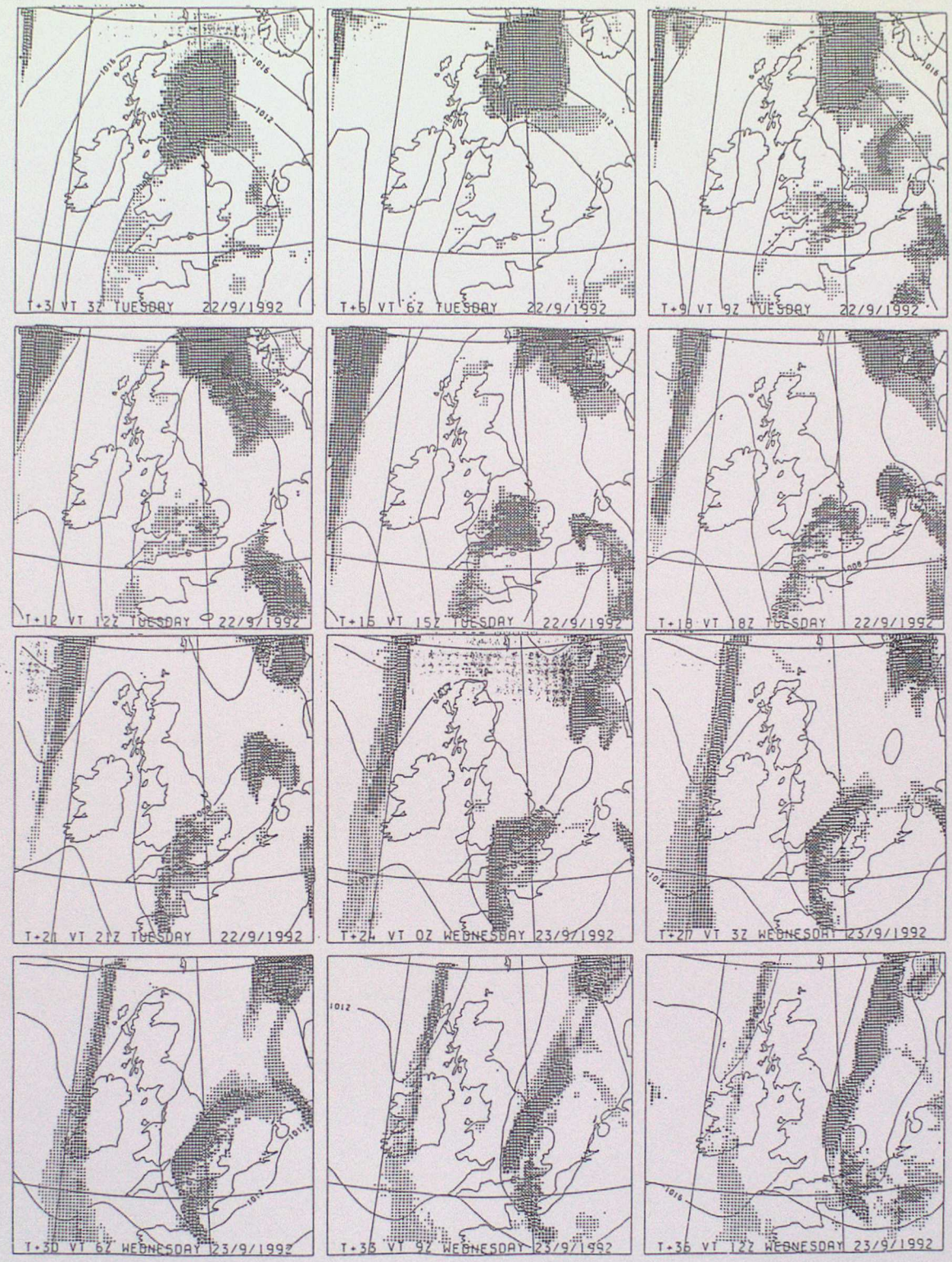

FIGURE A.10 Forecast precipitation and mean sea level pressure from NMM data time 06UTC 22 September 1992 at 3 hourly intervals from 03UTC 22 September 1992 to 12UTC 23 September 1992. Forecast R) in table A.1

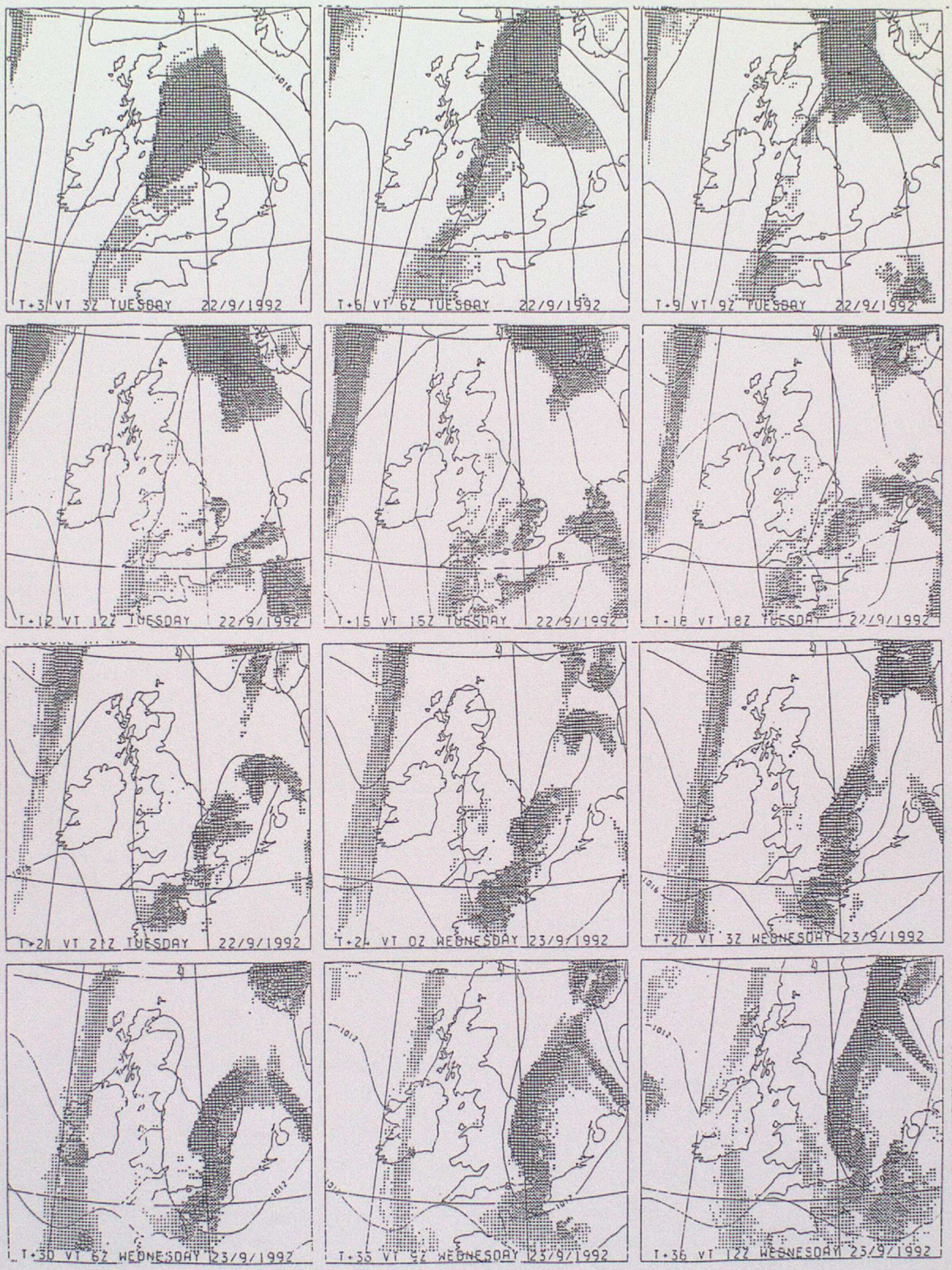

FIGURE A.11 Forecast precipitation and mean sea level pressure from NMM without data assimilation and intermediate convection parameters from 00UTC 22 September 1992 global analysis at 3 hourly intervals from 03UTC 22 September 1992 to 12UTC 23 September 1992. Forecast O2) in table A.2